TOPICAL REVIEW

Chemical sensor systems based on 2D and thin film materials

To cite this article: Charles Mackin *et al* 2020 *2D Mater.* **7** 022002

2D Materials

TOPICAL REVIEW

Chemical sensor systems based on 2D and thin film materials

Charles Mackin[1], Andrea Fasoli[1], Mantian Xue[2], Yuxuan Lin[2], Aminat Adebiyi[1], Luisa Bozano[1] and Tomás Palacios[2]

[1] IBM Research–Almaden, 650 Harry Road, San Jose, CA 95120, United States of America
[2] Massachusetts Institute of Technology, 77 Massachusetts Ave, Cambridge, MA 02139, United States of America

E-mail: charles.mackin@ibm.com and tpalacios@mit.edu

RECEIVED
17 July 2019

REVISED
13 November 2019

ACCEPTED FOR PUBLICATION
22 January 2020

PUBLISHED
12 February 2020

Keywords: graphene, artificial neural networks, metal oxide semiconductors, systems, chemical sensors, biosensors

Abstract

This review examines the advantages of two-dimensional (2D) and thin film materials in the development of chemical sensor systems. More specifically, this paper focuses on the use of graphene, transition metal dichalcogenides (TMDs), and thin film metal-oxide semiconductors (MOX) in gas- and liquid-phase chemical sensing applications. Key features in terms of material properties, device characteristics, as well as scalability for system development are examined. Key challenges associated with various sensing approaches (e.g. optical, electrochemical, FET/chemiresistive) are presented along with recent advances. Lastly, common methods for preprocessing and pattern recognition are summarized while highlighting the development of olfaction-inspired sensor systems to motivate the use of machine learning for data analysis.

1. Introduction

The chemical sensor market represents about 15% of the overall sensor market and is projected to expand from $18.6 billion in 2017 to approximately $28.2 billion in 2023, representing a compound annual growth rate (CAGR) of 7.2% [1, 2]. Although chemical sensors have found use in a variety of markets (e.g. food and beverage, agriculture, automotive), health care is anticipated to remain the largest segment and a key driver of growth. Well-known current applications include consumer glucose sensing for the management of diabetes mellitus as well as clinical hematology laboratories used by physicians as first-line indicators of overall patient health. In terms of emergent technologies, advances in chemical sensors are driving next-generation DNA sequencing with the aim of drastically reducing cost and sequencing times [3, 4]. This has potentially broad implications for cancer research [5], the study of infectious diseases [6], and may eventually allow genome sequencing to become accessible at the consumer level. In terms of future applications, chemical sensors may eventually give rise to entirely new markets through programs such as the National Institutes of Health (NIH) BRAIN Initiative, which aims to map the circuitry of the brain in large part through the development of better instrumentation (i.e. sensors) [7–10].

Owing to their high surface-to-volume ratio, two-dimensional (2D) and thin film materials are particularly promising in chemical sensing applications. This allows a large portion of their 'bulk' material properties to be modulated in response to chemical changes occurring at or near the surface, which generally leads to enhanced sensitivity. 2D materials have also uniquely benefited from years of sustained investment and research interest across a broad spectrum of fields spanning physics, materials science, chemistry, and engineering. As a result, 2D materials benefit from a particularly well-developed body of knowledge and level of maturity that places them at a potentially opportune moment for technology transfer to real-world applications and the broader sensor market. This is supported by the formation of a number of start-ups and commercial suppliers in recent years focusing on reliable wafer-scale materials synthesis and transfer processes potentially suitable for high-volume manufacturing while maintaining compatibility with conventional complementary metal-oxide semiconductor (CMOS) fabrication processes [11–13].

At the same time, the confluence of large datasets and advancements in computational hardware such as graphics processing units (GPUs) has spurred remarkable progress in data analysis and pattern recognition through the use of machine learning [18]. Machine learning is now finding uses in virtually every industry

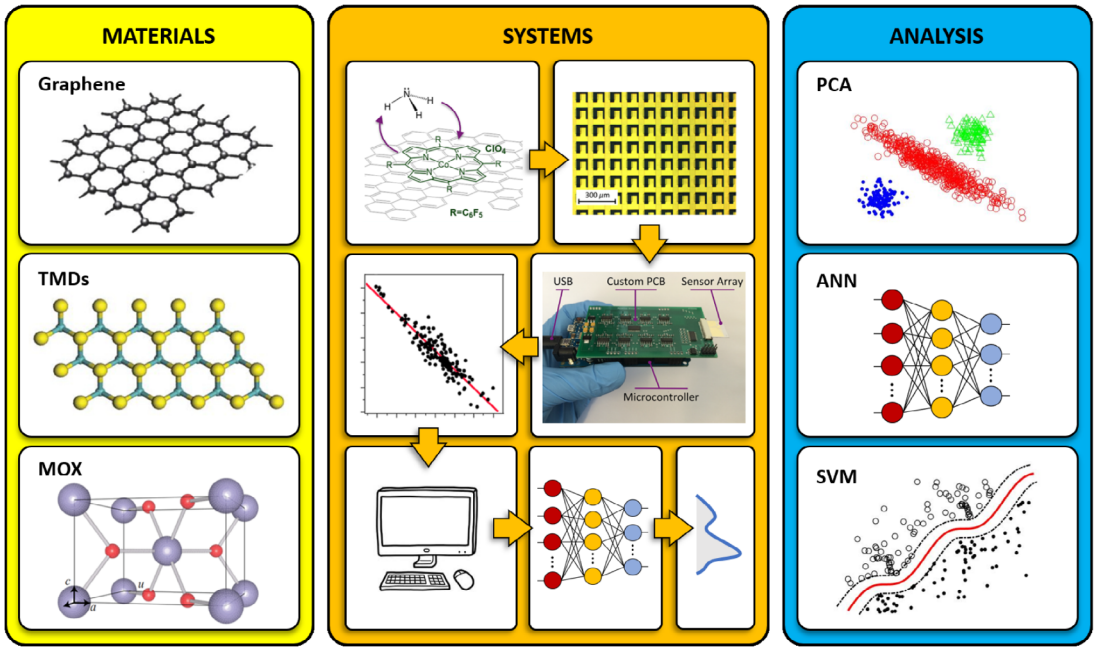

Figure 1. 2D and thin film materials are promising for sensing applications owing to their high surface-to-volume ratio. These materials may be functionalized and used to construct large-scale arrays of many specific (or partially specific) chemical sensors. Sensor systems designed to rapidly interrogate large-scale arrays generate a wealth of data, which when combined with analysis techniques such as machine learning, may be used to classify and analyze complex chemical environments. Graphene image reproduced from Scarselli *et al* [14], with permission form IOP Publishing; TMD image taken from Wu *et al* [15], copyright 2018 Elsevier; MOX image taken from Schleife *et al* [16], with permission from American Physical Society; sensor system images reproduced in part from Mackin *et al* [17], copyright 2018 Applied Materials and Interfaces.

from automotive [19] to health care [20, 21] to consumer electronics as a means to classify complex datasets and inform decision making in an increasingly data driven world. In some instances, these systems have even surpassed human capabilities [22–24]. Such analytical capabilities, when combined with multi-device sensor systems, enable advancements in the analysis of complex chemical environments. Although incorporation of machine learning in chemical sensing is not a novel concept, 2D materials and machine learning both appear to have reached inflections points—almost simultaneously in recent years—making this intersection of fields particularly interesting and promising.

A graphical summary of this review is presented in figure 1. While a plethora of 2D materials exist with potential applications to sensing, this review focuses on what are deemed some of the promising 2D and thin film materials with special emphasis given to device- and system-level challenges. This review is organized as follows: *section* 2 introduces select materials and summarizes key properties for chemical sensing applications. *Section* 3 provides an overview of the various types of chemical sensors along with their benefits and drawbacks. *Section* 4 provides a brief summary of key performance metrics to be considered in evaluating new and existing sensor technologies. *Section* 5 details advantageous features and recent progress in transitioning device-level chemical sensors to the system level. *Section* 6 summarizes various methods for data analysis while highlighting the benefits and advancements related to machine learning. *Section* 7 provides concluding remarks.

2. Survey of materials

This section surveys select 2D and thin film materials for use in chemical sensors. Two-dimensional sensing materials may be classified into three groups: semi-metals, semiconductors, and insulators. Graphene is the most promising and mature of the semi-metallic materials with transition metal dichalcogenides (TMDs) being the most promising of the semiconducting materials. The third group, 2D insulators, are not conducive to electrical readout in most applications and therefore outside the scope of this review. Lastly, thin-film metal-oxide semiconductors (MOX) are examined as promising candidates for use in chemical sensor systems.

Graphene possesses the highest surface-to-volume ratio of any the 2D materials in that every atom is a surface atom [25]. It also represents one of the most widely researched 2D materials [26] with many applications to sensing [27, 28]. Graphene was the last member of the low-dimensional carbon allotropes to be isolated in 2004—the other two being Buckminsterfullerene and carbon nanotubes. Graphene consists of a two-dimensional plane of carbon atoms arranged in a hexagonal lattice and represents the 2D building block for graphite, possessing strong in-plane carbon bonds and weak van Der Waals forces between layers. It possesses an atomic density of 3.82×10^{15} cm^{-2} and a

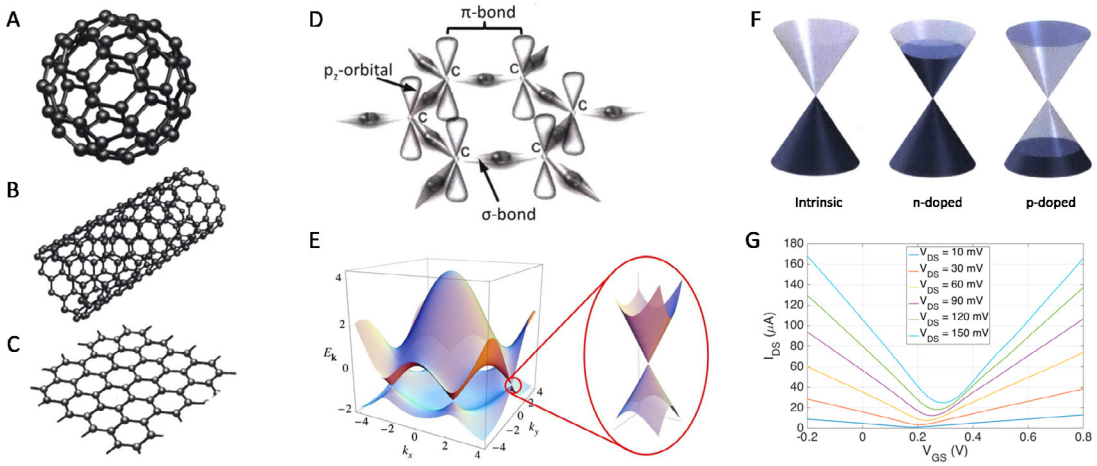

Figure 2. Low-dimensional carbon allotropes including (A) Buckminsterfullerene, (B) carbon nanotubes, and (C) graphene. (D) Graphene sp^2 hybridization depicting σ-bonds and π-bonds. (E) Band structure of graphene. (F) Low-energy band structure of graphene with Fermi levels indicated for various doping levels. (G) Graphene *I–V* Characteristic. Images (A)–(C) taken from Scarselli *et al* [14], with permission form IOP Publishing; image (D) taken from Schulz *et al* [45], copyright 2014 Elsevier; image (E) taken from Geim *et al* [46], with permission from Science; image (F) taken from Wang *et al* [47], copyright 2015 Springer Nature; image (G) taken from Mackin *et al* [48] with permission.

carbon-to-carbon bond length of 1.42 Å [29, 30]. Each carbon atom has four valence electrons that undergo sp^2 hybridization. Three of the four electrons form in-plane covalent bonds with the three nearest neighbors, termed sigma bonds (σ-bonds), which provide graphene with much of its mechanical strength. The fourth valence electron is oriented perpendicular to the plane in a p_z orbital and forms what are termed pi-bonds (π-bonds). These electrons are delocalized—enabling charge transport—and are what gives rise to graphene's electrical properties. Graphene also exists in multi-layered forms [31–35]. Monolayer graphene, however, tends to offer the highest sensitivity through its surface-to-volume ratio and will be the focus of this review. A brief overview of graphene's key material features is presented in figure 2.

Carrier transport within the π-bonds above and below the plane of carbon nuclei are one of the reasons graphene is particularly promising for sensing applications. These π-bonds are readily influenced by environmental changes and directly alter graphene's electrical properties to provide transduction—the means by which chemical signals are transformed into electrical ones. This provides graphene with innate sensitivity to many different environmental changes, which can be advantageous in some applications. For instance, transduction in graphene has been shown capable of detecting individual molecules [36]. In many cases, however, innate sensitivity also poses challenges in achieving selectivity, an equally important performance metric in many applications.

Graphene's low-energy band structure is unique in that valence and conductance bands meet at a single point, referred to as the Dirac point. This makes graphene a zero-band gap semiconductor or semimetal. This means that conductivity in graphene can be modulated when used as a sensor (like a variable resistor), but that graphene cannot be switched 'off' or placed into a non-conductive state. In addition, the linear dispersion in graphene's cone-shaped low-energy band structure is reminiscent of photons and gives rise to massless relativistic particles called Dirac fermions [37–41]. This allows charge carriers in graphene to move at potentially very high speeds termed the Fermi velocity, which is defined by the slope of the energy-momentum dispersion and is roughly 1/300 the speed of light [42–44]. This in turn allows for very high carrier mobilities, which may be useful in terms of both sensor response time and sensitivity.

Graphene's electrical, chemical, mechanical, and optical properties add to its promise as a sensing material. Graphene has been reported capable of carrier mobilities ranging from 50 000–200 000 $cm^2\ V^{-1}\ s^{-1}$ [49, 50]. These mobilities, however, typically only exist under highly constrained measurement conditions such as low carrier concentrations ($<5 \times 10^{11}\ cm^{-2}$), cryogenic temperatures (<5 K), and the use of specialized substrates or suspended graphene (i.e. no substrate). Under more practical conditions, graphene mobilities are typically reported in the range of 500–10 000 $cm^2\ V^{-1}\ s^{-1}$ and vary as a function of carrier type and concentration. In most cases, however, graphene's mobility remains universally better than the mobilities achieved in more conventional materials such as silicon [51–54]. These high carrier mobilities make graphene more responsive to environmental changes as a sensor. For instance, in the case of field-effect transistor (FET) sensors, sensitivity is partially defined by transconductance, $g_m = \partial I_{DS}/\partial V_{GS}$, which is directly proportional to mobility [55, 56]. High carrier mobility also translates into better frequency response characteristics, which leads to reduced signal attenuation in high-frequency (i.e. high-speed) operation [57–59]. Graphene also produces relatively low

noise, which may provide enhancements in signal-to-noise ratio (SNR) for sensing applications [60–62].

Graphene also has high chemical stability and is largely unreactive (i.e. inert) in a whole host of chemical environments [63, 64]. This finding should not be surprising as closely related glassy carbon electrodes have long been used as an alternative to highly inert but expensive platinum electrodes in electrochemistry. This high chemical stability enables graphene to form a direct (or more direct) interface in many different chemical environments allowing for enhanced sensitivity. This direct interface is particularly advantageous in electrolytic environments as it allows graphene to take advantage of the electric double layer phenomenon and resulting ultrahigh interface capacitance, which serves to further enhance sensitivity [65–70]. Graphene has also been shown to possess a wide electrochemical potential window in a variety of solutions including 2.5 V in phosphate buffered saline (PBS), which mimics physiological conditions [71]. This allows graphene to be directly interfaced with and gated through solutions, such as electrolytes, without inducing large interfacial leakage currents, which points to graphene's potential utility in biochemical sensing applications. Graphene's inertness also provides some level of bio-compatibility, with experiments by Hess *et al* showing no damage or preferential migration of neurons when cultured on graphene versus conventional silica substrates [72].

In terms of mechanical properties, the Young's modulus for graphene has been reported in the range of 1–2.4 TPa with a breaking strength of 42 Nm^{-1} [73, 74]. Graphene also provides innate flexibility due to its 2D structure [75–77]. These traits may enable the construction of flexible, stretchable, and foldable sensors [75, 78]. Graphene also provides low optical absorption, primarily due to its thinness, and appears largely transparent in the visible spectrum [64, 79]. This may prove useful in applications such as optogenetics where graphene may allow for optical stimulation of neurons, imaging, and electronic sensing to occur simultaneously with little interference [80–83].

It is important not to overlook the critical role played by synthesis techniques in providing a baseline of consistent and repeatable material properties for sensor fabrication. Graphene was initially, and often times still is, isolated through the repeated mechanical exfoliation of highly oriented pyrolytic graphite (HOPG) [84–86]. Graphene may also be grown epitaxially through the thermal decomposition of silicon carbide [87–89]. In this process, silicon carbide is annealed at high temperature—typically above 1000 °C—in an inert gas, which causes the silicon desorption and carbon bonding to form epitaxial graphene. Lower quality, multi-layered graphene films may also be synthesized through the reduction of graphene oxide [90–92]. Finally, graphene has also been successfully synthesized using chemical vapor deposition (CVD) [93–97]. In this process, methane is typically flown over a metal catalyst—usually a copper or nickel foil—at high temperature resulting in graphene formation on the metal surface. CVD is the most practical synthesis method as it is capable of producing large sheets with uniform material properties at relatively low cost—the cost of which may be potentially further reduced through the reuse of catalyst foils [98, 99].

The second category of materials covered in this review are 2D semiconductors, and more specifically transition metal dichalcogenides (TMDs). Bulk TMDs have been studied for decades and possess a variety of compositions [101]. Like graphene, bulk TMDs are layered materials with strong in-plane bonds and weak out-of-plane van der Waals bonds. The first discovery of layered TMDs was by Linus Pauling in [102] and the first production of monolayer MoS_2 suspensions were performed by Per Joensen in [103]. TMD materials consist of a transition metal layer, typically from groups IV–VII, sandwiched between chalcogenide layers. Most TMDs have an atomic ratio of 1:2 with chemical formula MX_2, where M is a transition metal (e.g. Mo, W) and X is a chalcogenide (e.g. S, Se, Te) [100, 104, 105]. Some special cases include 2:3 quintuple layers (M_2X_3) and 1:1 metal chalcogenides (MX) [104, 106, 107]. Depending on the atomic arrangement, TMDs have several distinct phases. The most common thermodynamically stable phases contain trigonal prismatic (hexagonal, 2H) or octahedral (tetragonal, T) metal atoms. Due to the diverse chemical composition and different phases, the electrical properties of TMDs may vary greatly. This review will focus on the most widely studied 2D TMDs—group VI transition metals Mo and W combined with dichalcogenides S and Se.

Depending on the different coordination of the metal atoms, 2D TMDs exhibit polytypic structures including trigonal prismatic (2H phase), octahedral (1T phase) and distorted octahedral (1T' phase) [108]. 1T and 1T' phases are metastable and tend to aggregate and transform into the more thermodynamically stable 2H phase [108, 109]. 1T and 1T' phases show metallic behavior due to degenerated $d_{xy,yz,xz}$ orbitals, which form a single, partially-filled band. With the trigonal prismatic structure, a bandgap is present between the filled d_{z^2} band and empty $d_{x^2-y^2,xy}$ band thus making the 2H phase semiconducting [110]. Figure 3(B) shows the band structure evolution calculated by density functional theory of 2H MoS_2 from a bulk indirect bandgap semiconductor to a monolayer direct bandgap semiconductor [100]. The bandgaps of 2D TMDs span a large range, including the entire visible spectrum and near infrared [96]. For monolayer MoS_2, the calculated bandgap is 1.71 eV while the experimental value is 2.16 eV [111]. Unlike graphene, the natural bandgap in 2D TMDs can be used to provide higher on/off ratios (i.e. switching behavior), greater signal amplification, and subthreshold operation. The ability to switch TMDs into a non-conductive state potentially enables the integration of 2D digital

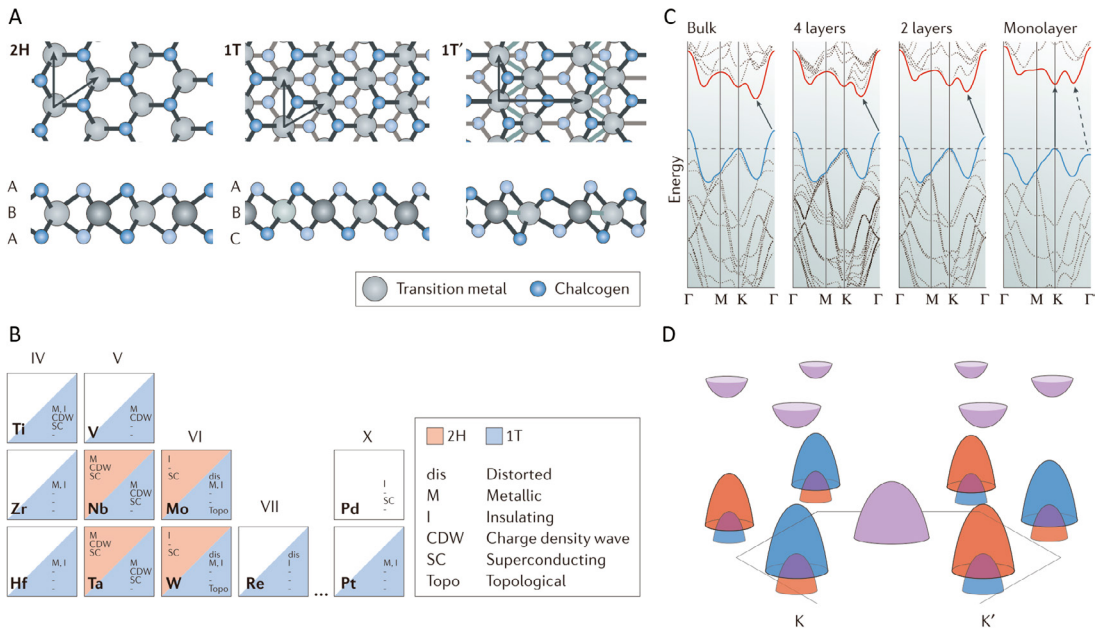

Figure 3. (A) Atomic structure for single layer transition metal dichalcogenides (TMDs) in the 2H, 1T, and 1T' phases, (B) periodic table of elements typically found in layered TMDs, (C) evolution of the band structure for 2H–MoS_2 with decreasing number of layers, and (D) the schematic representation of the band structure for 2H–MoS_2. This TMD overview image is reproduced from Manzeli *et al* [100], copyright 2017 Springer Nature.

electronics alongside 2D sensors all using the same material. Basic logic gates, the basis of more complex digital electronics, have already been demonstrated using several 2D TMDs [112–115]. This in turn may provide better scalability in terms of array design since individual sensors can be turned on and off for read-out through selector transistors. Operation in the sub-threshold regime can also lead to enhanced sensitivity through the conventional exponential dependence of current on the gate voltage in field-effect transistors (FETs) [116].

In addition to providing a natural bandgap, most 2D TMDs also exhibit high carrier mobility. The theoretical mobility of monolayer MoS_2 at room temperature ranges from 10 to 1000 $cm^2\ V^{-1}\ s^{-1}$ [117–119]. In practice, however, the mobility of 2D TMDs is strongly dependent on the cleanliness and maturity of the fabrication process as well as environmental factors such as surface absorbents and defects in the surrounding dialectic [100]. In order to mitigate mobility degradation, high temperature annealing in vacuum is often used to help remove surface absorbents and high-k dielectric encapsulation (e.g. HfO_2) may be used to screen Coulomb scattering [115, 120]. Through dielectric environment engineering, the experimental mobility of monolayer MoS_2 at room temperature has been reported close to 150 $cm^2\ V^{-1}\ s^{-1}$ [115].

TMDs also exhibit excellent mechanical properties making them potential candidates for flexible, wearable sensor systems [121]. The Young's modulus of few layer, freely suspended MoS_2 nanosheets have been reported as high as 0.33 ± 0.07 TPa [122]. Bertolazzi *et al* reported high in-plane stiffness and Young's modulus for single-layer MoS_2 of 180 ± 60 Nm^{-1} and 270 ± 100 GPa, respectively [122]. The high strength of 2D TMDs can also withstand strains up to 10% [123]. Calculations further suggest that tensile strains in semiconducting TMDs can be used to tune the band structure, charge carrier effective masses, thermal conductivity, and other properties [100]. The piezoresistive coefficient for monolayer and a few layer MoS_2 is also two orders of magnitude higher than that of graphene. With a much higher fracture strain (~11%) than silicon (0.7%) and comparable piezoresistive coefficient, MoS_2 and other 2D TMDs are exemplary candidates for the development of flexible sensors for non-planar surfaces and highly distorted objects such as biological tissue [100].

Similar to graphene, most 2D TMDs can be mechanically peeled off from their layered bulk crystals. The mechanically exfoliated thin flakes provide a quick and easy source of monolayer TMDs with good electrical, mechanical, and optical properties making them especially popular for proof-of-concept device demonstrations. This method, however, is not scalable or reliable for large-area sensor array fabrication. Some more scalable and practical approaches are molecular beam epitaxy (MBE), chemical vapor deposition (CVD), and metal-organic CVD (MOCVD). MBE generally requires the use of ultrahigh vacuum where molecular beams of the source material are deposited onto a heated substrate while carefully monitoring film thickness through electron diffraction [100, 124]. The quality of MBE films is highly dependent on the underlying substrate, with poor lattice matching resulting in polycrystalline films with high dislocation and defect densities [100]. CVD TMDs are most commonly synthesized by evaporating metal oxide

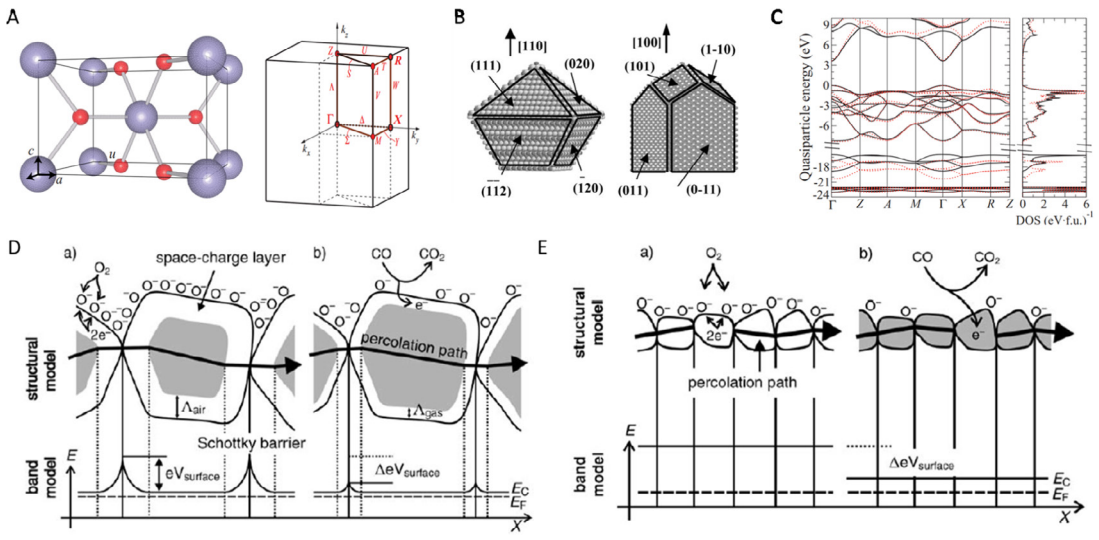

Figure 4. (A) Crystallographic structure of rutile SnO_2 and associated Brillouin zone. (B) Models of faceting of SnO_2 grains of different sizes deposited by spray-pyrolisis. (C) Simulated bandstructure of SnO_2. (D) Conduction model for MOX grains with $D > 2L_{SC}$ or (E) $D < 2L_{SC}$, in the absence or presence of reducing analyte. Images (A) and (C) taken from Schleife *et al* [16], with permission from American Physical Society; image (B) taken from Korotcenkov *et al* [131], copyright 2004 Elsevier; images (D) and (E) reproduced from Fanke *et al* [132], copyright 2006 Wiley.

and chalcogen precursors, which undergo a two-step chemical reaction that results in the formation of a stable TMD film on the surface of a substrate. This method does not require ultrahigh vacuum and tends to be more economical in achieving large-area synthesis of 2D TMDs [96, 104]. Point defects and multi-layer sites, however, are commonly present in CVD-grown films and often result in carrier mobilities below a few tens of $cm^2\ V^{-1}\ s^{-1}$ [118, 125]. MOCVD uses gaseous metal-organic or organic sources in which target atoms along with complex organic molecules are flowed into a chamber through mass flow controllers at a precise ratio. While the molecules decompose inside the chamber, target atoms may be deposited onto the substrate atom by atom [126, 127]. MOCVD can provide atomic scale deposition with morphological homogeneity of domain sizes and thicknesses but at a relatively slow growth rate and higher production cost [96, 104]. Overall the synthesis technology of large-area 2D TMDs with high yield, consistent electrical properties, and uniformity is still relatively immature. When compared to their mechanically exfoliated counterparts, most synthesized films experience reductions in carrier mobility, substantial doping, and inhomogeneity in film thickness. This may lead to sensors with reduced sensitivity, reproducibility, and reliability. In addition, some TMDs such as MoS_2, typically make use of seeding layers such as perylene-3,4,9,10-tetracarboxylic acid tetrapotassium salt (PTAS) [128]. This results in some synthesized TMDs being incompatible with water, a critical solvent in both microfabrication processes and eletrolytic sensing environments. This motivates advances in TMD synthesis without the use of water soluble seeds. It is also worth noting that unlike graphene, TMDs tend to have poor Ohmic contacts. Advances in this area have been made through the use of phase-change contacts, which slightly complicate fabrication processes relative to graphene [129, 130].

The final category of materials examined in this review is that of metal oxide semiconductors (MOX). The discovery that in some semiconductors, such as Ge or ZnO, exposure to different environments triggers a change in their surface electrical properties dates back to the 1950s [133, 134]. The first gas detecting devices based on this principle were reported in the following decade [135] and eventually commercialized as sensors for flammable gases [136, 137]. A wealth of MOX in a variety of forms and compositions have since been explored for the purpose of gas sensing [138]. This may lead to the expectation of a mature field wherein the primary challenges have been resolved and only incremental gains are possible. On the contrary, fundamental and applied MOX research continues to date, as new applications, made possible by recent advancements in miniaturization and power consumption of MOX-based devices, drive the demand for further breakthroughs in the form of improved sensing performance, access to a more diverse set of responses, suppression of spurious signals, and extended lifetime.

A range of binary and ternary combinations of metals with oxygen give rise to narrow- and wide-bandgap semiconducting materials [138]. Common examples includes SnO_2, ZnO, In_2O_3, WO_3, Fe_2O_3 and many others. By virtue of its high sensitivity to reducing gases and resilience to long-term changes in its electrophysical properties compared to other MOX, SnO_2 is by far the most widely investigated material and most commonly used material in commercial MOX sensors [139]. SnO_2 is a direct wide-bandgap (3.6 eV) semiconductor typically taking the rutile structure of casserite (figure 4(A)). The surface of each

crystallographic plane is associated with a different density of surface states, concentration of adsorbed species, as well as adsorption and desorption energies. This contributes to a dispersion of chemisorption behaviors in polycrystalline films and films expressing grains with different faceting [131] (figure 4(B)). While stoichiometric SnO_2 exhibits low conductivity as a consequence of its wide bandgap (figure 4(C)), nonstoichiometric SnO_2 possesses a high volumetric density of oxygen vacancies, which act as electron donor sites and dominate electrical transport properties making the material an n-type conductor [140].

The sensing mechanism in MOX can be illustrated as arising from the combination of receptor and transducer functions [141]. The receptor function corresponds to the interactions occurring at the gas-solid interface between a MOX grain and its surrounding environment. It has long been recognized that in oxygen-rich atmospheres such as ambient air, oxygen adsorbs on the surface of MOX. At elevated temperatures ($T \gtrsim 100$ °C for SnO_2), this adsorption process is accompanied by an exchange of electrons (chemisorption) which are trapped at the surface. This results in a surface potential barrier (0.5–1 eV [132]) and band bending associated with the formation of a space-charge region (electron-depleted), L_{SC}. The extension of L_{SC} into the grain is related to the Debye length L_D, which for SnO_2 is typically on the order of 3 nm [132]. Studies performed with infrared (IR) analysis, temperature programmed desorption (TPD), and electron paramagnetic resonance (EPR), established that at temperatures above ~150 °C molecular oxygen O_2 dissociates into atomic oxygen and that between ~150 °C and 500 °C the dominant adsorbed species is atomic O^-, which traps a single electron. At even higher temperatures, surface coverage is dominated by O^{2-}. The interaction of the surface with the environment is mediated by the oxygen coverage. SnO_2 sensors are typically operated in a range of 300–500 °C, where the concentration of adsorbed oxygen and the reaction rate promote enhanced sensitivity. In the case of a reducing gas, such as H_2, CO, or several volatile organic compounds (VOC), chemical reactions result in the release of the surface oxygen and, consequently, of the trapped electrons, which become available for conduction. At this point, the transducer function of the device takes place, as the released electrons travel through the material and, if collected at the electrodes, contribute to a measurable change in resistance.

The electric potentials experienced by electrons in MOX strongly depend on the morphology of the film and, more specifically, on the average grain diameter D [142]. Two primary regimes can be distinguished: for D greater than or comparable with $2L_{SC}$, the analyte interaction affects the charge density at the surface of the grain, while the bulk remains partly or mostly unaffected. In this scenario, the electron transport behavior is determined at the boundary of the grain (or agglomerate of grains), where a potential barrier can be established and modulated by the presence of the gas (figure 4(D)). Here, the extent of the grain-to-grain connection (neck) becomes relevant, as conduction through a thick neck ($t_{neck} \gg 2L_{SC}$) cannot be effectively modulated as well as through a thin one ($t_{neck} < 2L_{SC}$). Electrons generated during the interaction of the gas with the surface oxygen have to overcome multiple potential barriers before reaching one electrode. On the other hand, in the case of $D < 2L_{SC}$, a flat band regime is established, with grains that are fully depleted when the oxygen coverage is at its peak (figure 4(E)). The presence of an analyte then affects the conductivity of the full grain. Noticeably, injection at the Schottky barrier formed at the interface of the film with the electrodes becomes highly relevant to determine the transport properties of the sensing device.

On the basis of this conduction model, it becomes apparent that films comprising smaller grains are more effectively modulated than their larger grain counterparts and result in improved sensitivity. This prediction was experimentally confirmed [141, 143]. For deposition techniques providing a high thermal budget, growth of thicker films is associated with larger grain size [144]. In this case, deposition of thin films that are a few tens of nanometers in thickness is preferable. The rate at which gases diffuse throughout the film may also play a crucial role in determining the sensing performance. For example, a comparison of responses between thin (~50–300 nm) and thick (15–80 μm) films of undoped SnO_2 [145] produced entirely different dependencies of sensitivity on operational temperature. As the sensor response is probed over a range of temperatures, a characteristic bell curved is observed, its shape-defining parameters also depending on the film thickness, which can be interpreted in the context of a diffusion-reaction model [144–147]. The model posits a competition between gas diffusion into the film and its consumption on the grains surface. Such competition results in a reduced concentration of the gas species across the depth of the film. It should be noted that the diffusion-reaction model does not specifically account for changes in oxygen species and their surface coverage with temperature. Nevertheless, the qualitative behavior is well reproduced. According to this model, thin MOX films are once again favored in terms of sensitivity, especially for higher temperatures operation [147].

Various synthesis techniques may be used in the preparation of thick and thin films of SnO_2. These methods can be categorized as vacuum- or solution-based. The first category includes processes such as thermal evaporation, CVD, sputtering, laser ablation, and atomic layer epitaxy. Vacuum-based processes are typically best suited for the deposition of thin films with controlled physical properties. However, they are often associated with a need for expensive tools and, potentially, low throughput, which may pose a challenge for their practical application. On the other

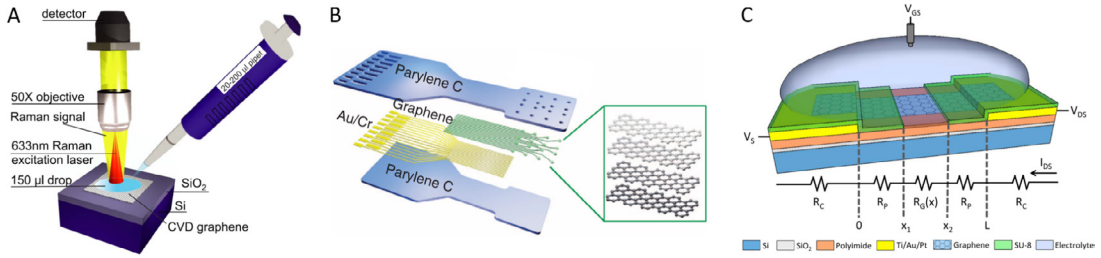

Figure 5. Chemical sensor types using 2D materials (A) optical sensors. (B) electrochemical sensors. (C) Field-effect transistor (FET) sensors. Chemiresistive sensors are structurally identical to FET-based sensors, except they lack a third electrode for gating the channel material. Image (A) taken from Paulus *et al* [151], copyright 2014 Springer Nature; image (B) taken from Park *et al* [80], copyright 2014 Springer Nature; image (C) taken from Mackin *et al* [152], copyright 2014 IEEE.

hand, solution-based methods can be cost effective and easier to deploy, but a narrow dispersion of physical properties can be harder to achieve. This second category includes processes such as sol-gel, spray pyrolysis, rheotaxial growth thermal oxide (RGTO), and the recently reported delayed ignition of combustion (DICO) [148–150].

Many deposition techniques for SnO_2 result in granular films characterized by extended mesoporosity (pores size between 2 and 50 nm). Such intrinsic porosity is advantageous as it allows the gaseous species to seep through the film and reach grains deeper into the bulk, so that the active area of the sensing film becomes much larger than its geometric planar area. Nevertheless, film thickness does play a role in the sensing performance, with thinner films being favored in terms of sensitivity and response time.

3. Chemical sensor types

Chemical sensors tend to fall within three categories: optical, electrochemical, or field-effect transistor (FET) based. Figures 5(A)–(C) provides a brief overview of the various chemical sensor types. Optical sensors are unique in that they potentially allow for analyte detection without adversely affecting the chemical environment. Optical sensors may also provide excellent selectivity in that analytes usually offer unique 'fingerprints' in the optical spectrum [151]. Various forms of light-matter interactions have been investigated for optical sensing including infrared absorbance of molecular vibrational modes, Raman scattering, and charge-transfer induced fluorescence quenching. These optical probes, however, often times suffer from weak signals or low sensitivity. As a result, larger analyte concentrations, sample volumes, and sampling periods are typically required. Incorporating 2D materials and other nanomaterials into the optical sensing paradigm can in many ways improve optical sensitivity.

There are two strategies typically involved in developing optical sensors using 2D materials. The first strategy is to enhance the spectroscopic response of the analytes by placing the 2D material in close proximity. This enhancement can be realized through couplings in either the optical domain or the electronic domain. One such example in the optical domain is graphene plasmon enhanced infrared vibrational spectroscopy. By exposing periodically patterned graphene nanoribbon arrays (~100 nm in width) to organic molecules in either a solvent-based or a gaseous environment, graphene plasmons in the mid-infrared (900–2000 cm^{-1} spectral range) may couple with various vibrational or rotational modes in the molecules [153–157]. Such couplings are characterized by plasmon-induced transparency, which gives rise to an enhancement factor of up to twenty relative to instances without graphene plasmonic structures [156]. Graphene-based plasmonic resonators may be further improved by hybridizing graphene plasmonic modes to metallic nano-antennas or critically coupled optical cavities [153]. Resonant frequencies of graphene-based plasmonic resonators can also be tuned widely through electrostatic gating [156]. This tunability provides a powerful lever in locally enhancing the spectral range of interest. Several studies have demonstrated graphene plasmonic sensors with sensitivities of 500 zeptomoles μm^{-2} for organic molecules such as polyethylene oxide (PEO) [154], and 800 zeptomoles μm^{-2} for gas molecules such as NO_2, N_2O, NO and SO_2 [157].

Couplings between 2D materials and analytes may also exist in the electronic domain, and may give rise to enhanced optical signals from the analyte as seen in methods like graphene enhanced Raman scattering (GERS) [158, 159]. Raman scattering spectroscopy signals from organic molecules have been observed to show enhancements of 2–17 times when placed in vicinity of graphene and other 2D materials [160, 161]. This enhancement is attributed to the hybridization of π-orbitals between graphene and the analyte along with significant charge transfer [158, 159]. Although improvements in sensitivity are generally limited in Raman scattering techniques, the enhancement effect in GERS provides both uniformity and repeatability and has been used for a variety of chemical and macromolecular sensing applications [159].

The second strategy is to harness special optical responses of the 2D materials that can be tuned widely through the physio-adsorption of analytes. For instance, the photoluminescence intensity of graphene

oxide (GO), MoS_2, $MoSe_2$, and WSe_2 can be modified by orders of magnitude when different gas molecules (O_2 and H_2O) [162], organic molecules (NADH, F_4TCNQ, and various organic solvents) [163–165] or macromolecules (peptides, proteins and DNA) [166] are physically adsorbed on the surface. This in turn can be readily characterized using a conventional fluorescent microscopy and used to quantify analyte concentrations. Although considerable progress has been made in scaling optical sensors and incorporating 2D materials for chemical applications [166], major challenges remain including material non-uniformities and limited reproducibility. In addition, optical sensors tend make miniaturization and the development of low-cost systems difficult as they require bulky and expensive apparatus such as light sources, microscopes, spectrometers, and optical filters.

Electrochemical sensors, as the name implies, quantify analyte concentration by inducing analyte migration near an electrode surface and by measuring the resulting current or voltage. These measurements are typically taken with respect to a reference electrode in order to provide both a stable and known reference potential. Common reference electrodes include Ag/AgCl and saturated calomel electrodes. In cases where reference electrodes are too costly or provide inadequate miniaturization, other materials may be employed as pseudo-reference electrodes with the aim of ensuring a known and stable interface potential at the reference. Ensuring known and stable interface potentials at all interfaces other than the sensor-analyte interface is fundamentally what allows changes in electrochemical measurements to be attributed wholly to chemical interactions occurring at the sensor-analyte interface.

Electrochemical sensors generally come in two varieties: Faradaic and non-Faradaic. Faradaic sensors quantify analyte concentration by reacting the analyte at the surface of an electrode via a reduction-oxidation reaction and by measuring the resulting electron transfer. Because Faradaic sensors measure analyte concentrations through reactions, they actively consume the analyte. This can introduce complex concentration gradients near the site of the reaction, which in turn can affect the rates at which new analyte, reaction byproducts, and other substances are carried to and from the electrode surface [167]. Faradaic sensors must also ensure the analyte being measured possesses the lowest oxidation-reduction potential to avoid its signal being overwhelmed by the reduction-oxidation reactions of other species. If the chemical environment does not allow for this, it may further complicate the sensor chemistry as the analyte may first need to undergo several reactions in order to be converted into another compound with a lower oxidation-reduction potential. Faradaic reactions are also 'destructive' measurements by nature in that they consume and potentially alter the analyte concentration through measurement. This can pose issues when monitoring analyte concentrations continuously over prolonged periods of time, especially at small volumes. In some cases, the reactive nature of these sensors may also produce undesirable and potentially harmful byproducts, especially in biochemical sensing applications.

Non-Faradaic electrochemical sensors, on the other hand, do not rely on reduction-oxidation reactions and typically quantify analyte concentrations via interface potentials or capacitive effects. In both cases, electrochemical sensors offer a high degree of precision in quantifying analyte concentrations because high-precision off-the-shelf electronics (e.g. ammeters, analog-to-digital converters) are readily available at low cost and because electron migration can be directly related to analyte concentration. Electrochemical sensors have been developed using a number of 2D materials and shown effective at measuring a variety of analytes. Although by no means an exhaustive list, some notable sensor types include electrolyte sensors [168, 169], neurotransmitter sensors [170–178], and electrophysiology sensors [179, 180]. The main setback, however, for electrochemical sensors in sensor systems is that they are electrode-based. Electrode-based sensors offer the benefit of simple construction, but are limited in terms of scalability because they typically require one readout wire for every sensor.

Field-effect transistor (FET) sensors aim to combine the benefits of electrochemical sensors with the scalability of complementary metal-oxide semiconductors (CMOS). This is achieved by having the sensing mechanism occur transversely to the readout mechanism, which is typically current based. FET-based sensors, as shown in figure 5(C), are typically comprised of three terminals: a source, drain, and gate. Source and drain contacts are used to facilitate the passage of current through the channel material. The gate electrode is then used, in the case of solution-based sensing, to bias the sensor in a particular region of the I–V characteristic. The sensing mechanism, similar to gating, occurs transverse to the channel region. Changes in analyte concentration then act to modulate the baseline current passing through the sensor as established by the gate bias. This sort of decoupling between sensing and readout mechanisms when combined with some basic principles from electrical engineering, allow FET-based chemical sensors to be scaled into large arrays in ways that electrode-based electrochemical sensors cannot. Unlike electrochemical approaches, FET-based sensors may also be used as amplifiers to provide pixel-level amplification [48, 58, 181, 182].

In some cases, FET-based chemical sensors may include an additional terminal for 'back gating'. In this case, a fourth terminal is fabricated, typically underneath the channel, to provide added flexibility in biasing the sensor. Another type of sensor, chemiresitive sensors, are simply a two-terminal variant of FET-based sensors in which the gate electrode has been removed. Gate electrodes may not be necessary

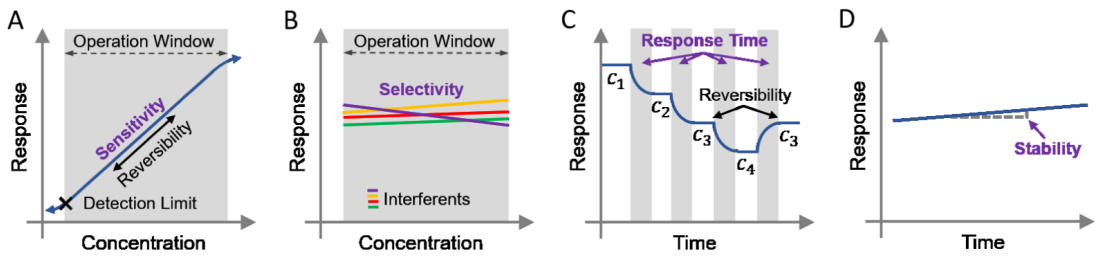

Figure 6. Overview of common sensor performance metrics: (A) Sensitivity including reversibility and window of operation, (B) Selectivity with respect to a number of interferents, (C) Response time from exposure to varying analyte concentrations, (D) Stability of sensor response over time.

for biasing in some liquid-phase sensing applications where the sensor may be doped through fabrication to operate in particular conductivity regime. Chemiresistive sensors are also particularly common in gas-phase sensing where gating through insulating gases is ineffective. In these cases, chemiresistive sensors can still be thought of as FET-based sensors that are 'gated' with respect to the ambient environment or vacuum potential. A variety of FET-based chemical sensors have been developed using 2D materials [183] including pH sensors [184], hydrogen peroxide sensors [185], glucose sensors [186], electrophysiology sensors [187], macromolecular sensors for DNA and prostate specific antigen (PSA) [188, 189], and chemiresistive sensors for the detection of ammonia [17].

4. Sensor performance metrics

The overall performance of a sensor is determined by a variety of factors, each of which may carry a different weight depending on the user-specified needs and operating environment. It is the combination of these performance metrics that determines the overall viability of a sensor (and system) as well as the potential scope of its application. This section details each of what are typically considered core performance metrics: sensitivity, selectivity, response time, and stability (figure 6). We emphasize this more holistic viewpoint of performance because new sensing technologies, even if capable of record performance in one metric, may not find use if lacking in one or more other metrics. A number of additional, or 'secondary' considerations may also exist when evaluating the overall performance or viability of a sensor. These may include shelf life, cost, manufacturing complexity, operating temperature, and power consumption. This review is not intended to be an exhaustive review of performance metrics, but to provide a holistic viewpoint of key factors and bring attention to the overall complexity involved in evaluating sensor performance.

Perhaps the most intuitive and frequently reported sensor metric is sensitivity. Sensitivity is a differential metric that aims to quantify the degree to which a sensor responds—however that is defined—to some change in analyte concentration. Sensitivity may be quantified in many ways depending on the application and sensor type. Some sensors produce a linear responses (i.e. constant sensitivity) over a broad range of analyte concentrations. Other sensors, such as ion-selective electrodes, might produce logarithmic responses (e.g. mV/decade) due to the physics governing interface potentials described by the Nernst equation [190, 191]. MOX sensor response is typically described by a power law, stemming from the dependence of the sensor resistance R on the partial pressure P of the target gas ($R = aP^n$, with $n \sim -1/2$ for detection of reducing gases by an n-type MOX such as SnO_2). Some sensors, such as nanowire FET-based pH sensors, have even been shown to produce exponential responses to changes in analyte concentration [192]. Linear responses are typically easiest to work with, but readout circuitry can be readily adapted to linearize both logarithmic and exponential responses. It is important to note that linear, logarithmic, and exponential sensitivities—which are described by simple mathematical models and can readily be related back to analyte concentrations—only hold for a limited range of analyte concentrations or window. For many applications, it is critical that this window encompass the range of analyte concentrations being measured (figure 6(A)).

In the case of FET-based sensors for liquid-phase applications, sensitivity can be thought of as the combination of two effects: the modulation of the gate voltage V_{GS} with respect to changes in analyte concentration C (i.e. $\partial V_{GS}/\partial C$), which is determined by the functionalization or in some cases innate sensitivity of the material; and the transconductance g_m (i.e. $\partial I_{DS}/\partial V_{GS}$), which describes the sensitivity of the readout current to modulations in the gate voltage. In optimizing sensitivity, the first factor is improved primarily through functionalization chemistry. The second factor, transconductance, is a standard FET parameter determined by factors such as with width-to-length ratio, carrier mobility, and gate capacitance. Additional factors influencing sensitivity might include contact resistance and velocity saturation. Sensitivity is also closely related to the detection limit, which describes the minimum discernible analyte

quantity and is typically limited by functionalization chemistry, the intrinsic noise of the sensor material, and various forms of electronic noise arising from the measurement system.

Selectivity aims to quantify sensor response (or lack thereof) to substances other than the analyte (figure 6(B)). Although not reported as often in literature, selectivity is equally important in many applications. For instance, a new sensor may exhibit record performance in sensitivity, however, absent selectivity, the sensor will be prone to misclassifying analyte concentrations in the presence of interfering compounds. In these cases, limitations in selectivity can be overcome by extracting (i.e. purifying) the analyte from its more complex originating chemical environment. This has the effect of shifting the complexity associated with developing a selective sensor into the sample preparation phase. In most cases, it is desirable to have the sensor selectively bind to the analyte despite a number of potential interferents. In the absence of innate material selectivity, this is achieved (like sensitivity) by functionalizing the surface of the sensor. These functionalizations can be rather complex and can involve a number of intermediate steps in cases where the functional molecule cannot be bound directly to the underlying 2D material. Because selectivity is difficult to know for an exhaustive list compounds, it is typically quantified for a limited number of interferents typically present within the sensing environment or use case. These interferents can be as common as water adsorption due to changes in relative humidity, which makes selectivity an important metric in determining the practicality of new sensors.

Fortunately, 2D materials such as graphene have benefited from the development of a variety of covalent and non-covalent functionalization chemistries [193]. The distinction between covalent and non-covalent functionalizations is especially important for 2D materials. Covalent functionalizations may couple more strongly to the 2D material and provide enhanced sensitivity, but may also disrupt (or degrade) carrier transport in the material, which counteracts sensitivity. Non-covalent functionalizations, on the other hand, provide weaker interactions with 2D materials but are more likely to leave the electronic transport properties intact. There also exist many other broadly applicable, mature, and selective bio-inspired synthetic compounds that may be used to provide selective sensitivity. Porphyrins, for example, perhaps best known for their role in allowing red blood cells to selectively bind to oxygen, have been extended to sense a variety of different compounds including aromatic compounds such as ammonia [17]. Ionophores, perhaps best known for their use as antibiotics and for selectively binding ions to disrupt cellular transmembrane potentials, have also been extended to selectively sense a variety of different ions including heavy metals [194]. A variety of biologically-derived antibodies also exist, which may be used to functionalize sensors to provide high levels of selectivity.

MOX are typically regarded as not highly selective, as their surface tends to interact with a large range of molecules when operated at high temperatures. Nevertheless, distinct reaction pathways and reaction rates can in principle be accessed throughout a range of temperatures, which may serve as a basis for discrimination of target molecules. This is the rationale behind temperature modulation of MOX sensors [195]. Periodic temperature cycling has been shown to be effective in improving capabilities of gas discrimination [196–198]. In addition, doping has also been utilized to enhance selectivity towards particular gas species [141, 199]. Two mechanisms allow dopants to affect selectivity, as well as sensitivity: chemical sensitization, where an exogenous impurity located at the surface of a MOX grain catalyzes chemical reactions or acts as a preferential adsorption site for the analyte; and electronic sensitization, where the presence of surface additives modify the extent of the surface depletion layer, typically extending it further into the grain through the formation of an additional Schottky barrier. Both pathways may be used to affect the extent by which MOX conductance is modulated in the presence of analytes and represent additional knobs in the tuning MOX properties to generate more diverse responses. Enabling such capabilities is key in developing sensor systems, which can leverage orthogonal responses of multiple sensing elements to identify complex odors by means of unique pattern attribution (section 6).

Response time quantifies how quickly measurements can be taken to reliably quantify the analyte after a change in concentration (figure 6(C)). Response time, as a result, limits the sampling rate that can be applied to a sensor and is critical for high-speed or high-throughput applications. A number of factors determine the overall response time of a sensor. Reaction kinetics between the analyte and sensor (i.e. forward and reverse reaction rates) form the basis for determining the rate at which the sensor reaches equilibrium. Reaction kinetics also determine the reversibility of the sensor response (i.e. does it respond equally to increasing and decreasing analyte concentrations). The presence of forward-only reactions hampers reversibility, which may not be critical, however, depending on the application. Response time may be further influenced by mass transport characteristics such as migration, diffusion, and in some cases convection. In some high-speed sensing applications like neural electrophysiology, where sample rates in excess of 20 kHz are typical, special care may be needed to ensure device characteristics such as parasitic resistances and capacitances do not limit response times [48]. For instances in which equilibrium cannot be reached within a suitable period, sensor response times may be truncated—using amperometric techniques,

for instance—while still accurately quantifying analyte concentration. This is a commonly used technique in consumer glucose monitors [200, 201]. In this case, analyte concentrations are approximated based on how rapidly the sensor responds before reaching equilibrium. These sorts of measurement techniques are analogous to approximating the distance an object will travel by measuring its velocity at a specific location.

Stability quantifies changes in sensor response with respect to time given that the analyte concentration and all other measurement conditions remain unchanged (figure 6(D)). This metric is used to determine the duration for which a sensor can be used after calibration and how frequently a sensor must be re-calibrated in order to maintain reliable readings. The importance of stability depends on the accuracy required for a given application, but tends to become especially important for sensors with logarithmic responses as even small degrees of instability over time produce large measurement inaccuracies. This important metric should not be overlooked, particularly in FET-based sensing approaches. Issues with stability have hampered the commercial viability of ion-selective field-effect transistors (ISFETs) for years. In the absence of issues associated with drift, however, these platforms allow for tremendous scalability with some commercial chips now containing upwards of a million sensors [3].

Stability is ensured first through the general chemical stability of all materials used to construct the sensor. This motivates the development of reliable synthesis techniques for TMDs that do not rely on water-soluble seeding layers [128]. Sensor stability may be further enhanced through the use of inert encapsulations or diffusion barriers to prevent the in-diffusion of contaminants that may dope and alter electric properties over time. Sensor stability implies the stability of all interfaces within the sensor and measurement path as well. This includes interfaces of the same phase (e.g. metal-semiconductor) and interfaces between phases (e.g. semiconductor-electrolyte). Common interfaces for FET-based sensors include the channel-substrate interface, channel-functionalization interface, and the interfaces between the channel and the source and drain contacts. A stable reference or pseudo-reference electrode is critical as well, meaning that all interfaces within the reference electrode must be stable. Only when all other interfaces are stable, can changes in sensor response be wholly attributed to the sensor-analyte interface and used to accurately quantify analyte concentration. By extension, in the absence of changing analyte concentration, the sensor should exhibit perfect stability. Of course no sensor is ideal, and all materials eventually react with their environment—albeit at different rates—given enough time. A variety of interactions may take place at any given interface and compete to determine the overall interface potential. Stability is then generally achieved by having one dominant interaction such that it wholly defines the interface potential. In the absence of a dominant interaction, interface potentials may be determined by a combination of weaker interactions that cannot be guaranteed to be stable such as the migration of impurities and contaminants. As a result, one or more interface potentials may drift over time, leading to instability in the overall sensor response.

Long-term stability is a challenge faced by MOX sensors as well. Although the lifetime of commercial MOX sensors are typically measured in years, responses are not expected to be constant with time but to progressively degrade. Sources of irreversible drift in both baseline conductance and response to analytes include structural transformations, phase transformations, poisoning, and device degradation [202]. In particular, grain growth and merging is particularly prominent in small-grain films [199]. Use of specific dopants, such as V and Re, was found to be effective in improving the stability of SnO_2 sensors [203]. It is believed that some additives, when present at the surface of the metal oxide main phase, can partially inhibit grain inter-diffusion thus limiting crystallite growth and improving structural stability [199]. However, it appears the effect does not generalize well to other dopant species. In addition, doping close to the solubility limit of the dopant into the MOX may result in the progressive segregation of the dopant to the surface, which may contribute to signal drift over time and, for sufficiently high doping levels, may generate undesired conduction pathways in the film structure [202, 204]. Overall, the effect of dopants on the long-term stability of MOX sensing films appears to be understudied and more work is needed in this area.

5. Multi-device sensor systems

There are typically two approaches in developing sensor systems for analyzing complex chemical environments, both of which motivate the development of multi-device sensor systems. One approach is to combine many 'orthogonal' sensors, each of which exhibits high selectivity and is responsible for quantifying a single analyte. This approach benefits from providing a known degree of accuracy in quantifying each analyte. For highly complex and unanticipated chemical environments, however, this approach may suffer from blind spots, or the inability to provide useful information on a number of analytes for which no selective sensors exist. From a manufacturing standpoint, it also becomes increasingly difficult to introduce thousands (or even millions) of different functionalization chemistries into a single sensor array. The second approach is then to develop systems that combine many less specific sensors, and through data processing techniques achieve a more comprehensive depiction of the chemical environment. These sorts of cross reactive sensor platforms typically rely on fingerprinting (i.e.

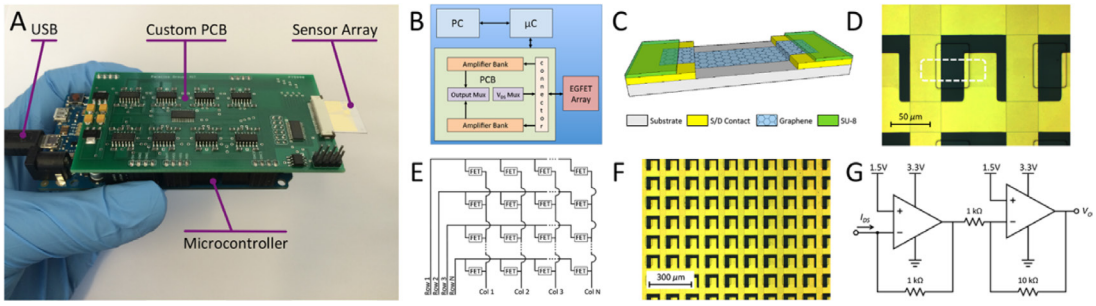

Figure 7. (A) Graphene micro-array sensor system that can be used as FET-based in liquid-phase sensing applications [206] or chemiresistive in gas-phase sensing applications [17], (B) overview of system-level integration, (C) individual graphene sensor structure, (D) optical microscope image of microfabricated graphene sensor, (E) sensor array architecture without selector transistors, (F) microfabricated sensor array, and (G) transimpedance amplifier for signal readout. Images reproduced from Mackin *et al* [17, 206], copyright 2016 Royal Society of Chemistry and 2018 Applied Materials and Interfaces.

a unique response to an analyte or class of analytes) and machine learning to associate complex chemical mixtures with certain odors or tastes [205]. This approach also enables more ubiquitous platforms for use across multiple application domains.

Irrespective of the approach used in analyzing complex chemical environments, FET-based sensors offer the unique advantage of combining the sensing capabilities of electrochemical sensors with the scalability of CMOS into an overall compact form factor (figure 7). This stems from the fact that the sensing mechanism in FET-based sensors, similar to gating, occurs transverse to the channel region (with the same being true for chemiresistive sensors). Changes in analyte concentration then act to modulate the baseline current passing through the sensor. This sort of 'decoupling' between the sensing and readout mechanisms allows FET-based chemical sensors to be scaled into large arrays in ways that electrode-based electrochemical sensors cannot. For instance, electrode-based chemical sensors require $M \times N$ readout wires to connect to an array of $M \times N$ sensors. FET-based chemicals sensors, on the other hand, may enable the readout of $M \times N$ arrays using only $M + N$ wires—with the use of 2D semiconducting materials enabling the fabrication of embedded selector devices within the sensor array. The difference in scalability becomes particularly important when developing arrays with more than several hundred sensors. The organization of FET-based sensor arrays along with the principles governing scaling and readout can be borrowed directly from architectures developed for dense memory circuits such as dynamic random access memory (DRAM) [207, 208]. Figure 7 depicts such a FET-based sensor system where a 16×16 sensor array may be interrogated using 32 (as opposed to 256) access wires. Figure 7, which happens to make use of graphene as the 2D material, is intended only as an illustrative example to highlight the advantages FET/chemiresistive sensor systems in terms of scalability. Similar systems could be readily be implemented using other materials such as TMDs and MOX [209–211].

Another important milestone in transitioning individual sensors to multi-device sensor systems, is the development of accurate device models. Electronic device models enable the rapid exploration of design variables and allow for application-specific performance optimization. Accurate device models also play a critical role in the design of readout circuitry. This includes appropriately matching the output impedance of the sensor with the input impedance of subsequent amplifier circuits. Device models capturing parasitic resistances and capacitances play an important role in the design of filter circuits used to avoid aliasing before digitizing sensor signals using analog-to-digital converters (ADCs). Development of accurate electronic device models, however, requires a thorough understanding of chemical interactions with the sensor and electronic transport properties in the underlying material. In some cases, complex features within the device model may need to be approximated or fitted using non-physical models to arrive at compact models compatible with conventional circuit simulators. To date, a plethora of characterization data, device models, and theory around operational mechanisms exist for graphene FETs and graphene FET-based sensors [17, 48, 152, 212, 213], TMD FETs and TMD FET-based sensors [214–218], as well as MOX transport characteristics and chemiresistive sensors [142, 219–221].

6. Data analysis

The use of multi-device sensor systems to detect and analyze complex environments can be applied to a variety of areas related to signal perception. Hardware systems have been developed to emulate biological tactile, auditory, visual, olfactory, and gustatory systems [222]. Tactile, auditory, and visual systems, however, tend to make use of force and optical sensors and are beyond the scope of this review. Chemical sensors, on the other hand, are most prevalent in hardware systems emulating olfactory and gustatory systems. These are commonly referred

Table 1. Overview of popular methods for data compression/feature extraction, cluster analysis and model classification. These techniques assume that raw data is preprocessed using fractional, relative, differential or other methods. Dimensionality reduction refers to data compression or additional feature extraction methods to further remove redundancies and to improve processing efficiency. Cluster analysis refers to unsupervised methods for exploration or classification of data. Classification models can either be for supervised or unsupervised methods of data analysis. Green denotes high frequency of use and straightforward implementation, yellow denotes possibility for use but not very frequent or straightforward and red signifies low frequency of use for sensing datasets.

	DIMENSIONALITY REDUCTION	CLUSTER ANALYSIS	CLASSIFICATION MODEL
PARAMETRIC			
PARTIAL LEAST SQUARES REGRESSION	🔴	🟡	🟢
PRINCIPAL COMPONENT ANALYSIS (PCA)	🟢	🟢	🟢
ANALYSIS OF VARIANCE (ANOVA)	🟡	🟢	🟢
LINEAR DISCRIMINANT ANALYSIS (LDA)	🟢	🔴	🟢
k-MEANS CLUSTERING	🟢	🟢	🟡
HEIRARCHICAL CLUSTERING	🔴	🟢	🟢
t-DISTRIBUTED STOCHASTIC NEIGHBOR EMBEDDING (t-SNE)	🟢	🟢	🟡
NON PARAMETRIC			
k-NEAREST NEIGHBORS (k-NN)	🔴	🟡	🟢
ARTIFICIAL NEURAL NETWORKS (ANN)	🔴	🔴	🟢
SUPPORT-VECTOR MACHINE (SVM)	🔴	🔴	🟢
DECISION TREES (RANDOM FOREST)	🔴	🔴	🟢

to as 'electronic nose' and 'electronic tongue' systems. The differences between electronic nose and tongue systems tend to be the type of sensors used and the phase of the analyte, with data preprocessing and analysis portions of the systems often times bearing many similarities. This review summarizes preprocessing and pattern recognition techniques common to both approaches and provides specifics related to olfactory-inspired hardware systems to motivate the use of machine learning with the understanding that many of these concepts also translate to gustatory sensor systems.

The techniques typically employed to analyze the sensor data vary mainly in the preprocessing and pattern recognition stages, depending on application and system constraints [223]. In the preprocessing stage, features, namely salient information representing sensor response to the analyte in question are extracted from sensor response curves. Depending on system stability and operation complexity, baseline manipulation methods may be employed. Assuming traditional sensor operation, this mainly involves steady-state sensitivity calculations for each sensor in the array as defined by a fractional baseline manipulation calculation—such as $\Delta G/G_0$, where G represents conductivity. The use of self-normalization and other baseline correction techniques has helped eliminate concentration dependence involving analytes like alcohol that elicit strong sensor responses [224, 225]. A basic guide of popular methods is outlined in table 1. It should be noted, however, that this review is not intended to be an exhaustive tutorial on the analytical methods themselves, but rather a presentation of—and motivation for—popular strategies that can be used in multi-device sensor systems. For an in-depth overview of algorithms and methods, the reader is encouraged to refer to analytics-specific reviews, where these strategies have been outlined in detail [226, 227].

Pattern recognition methods that include feature space visualization and compression are routinely used in conventional data classification, but have also proven useful for exploratory analysis and sensor performance feedback. Methods like principal component analysis (PCA) and linear discriminant analysis (LDA) map n-dimensional vectors into lower order feature spaces and expose colinearity of sensors, which minimizes the variation needed in building a sensor fingerprint (i.e. a unique response to an analyte or class of analytes). As such, genetic algorithms and other feature subset selection techniques have become more popular in determining the minimum combination of sensor information necessary for accurate classification [228, 229].

A more in-depth examination of olfactory-inspired sensor systems motivates the use of machine learning, and more specifically, artificial neural networks for data analysis. The concept of a sensor for olfaction was first introduced in 1982 by Persaud and Dodd [230]. Their research sought to emulate olfactory neuronal pathways (figure 8) and show that fine odor discrimination could be achieved with an array of partially specific chemosensors, rather than highly specific ones. Using three commercially available Figaro sensors to analyze eight odorants or volatile organic compounds (VOCs), they showed that the multi-device sensing pattern or fingerprint was reproducible over time. They analyzed the response ratio from these broadly-tuned detectors, and saw that unique odors occupied distinct points in multidimensional space. And so began a shift in focus from just improving sensing materials, to also incorporating data analytics and pattern recognition techniques to fingerprint odors much like the olfactory system.

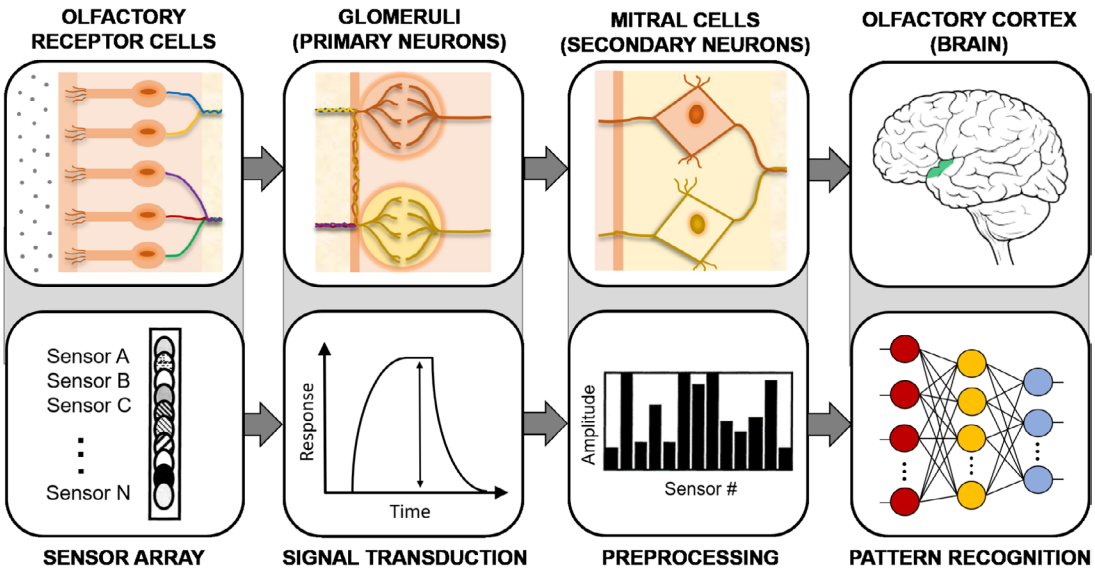

Figure 8. Parallel schematic comparison of mammalian olfactory system to an 'electronic nose' sensor system. Sensory information is transmitted from primary neurons and filtered through secondary neurons before decoding occurs in the olfactory cortex. Similarly, with these sensor systems, incident volatile compounds are transduced by the sensor array and signals are preprocessed before pattern recognition techniques are used to associate patterns with odors.

Not long after, the idea of olfactory coding was proposed by Schild [231]. It highlighted the neurobiology of evoked stimulus responses in olfactory receptor cells using vector spaces. It represented model-fitting of what these sensors, and more specifically electronic noses, seek to aspirationally replicate—similar to how convolutional neural networks (CNNs) take inspiration from the pioneering work by Hubel and Wiesel on the visual cortex [232]. Using information theory, the signal information processing flow was mapped from olfactory response cells to glomeruli and ultimately mitral cells within the olfactory bulb. Through this mathematical model, Schild showed how high selectivity could be achieved in the olfactory bulb through sets of mitral cells serving as mutually inhibited filters. This confirmed that low selectivity at the receptor cell level may be overcome by the neural network following that stage—and the power of these sensor systems would lie in the signal processing or the decoding of generated fingerprints beyond the sensor level.

Sensors for olfaction eventually moved toward a formalized definition in the 1994 review article by Gardner [233], where an electronic nose is defined as, 'an instrument, which comprises an array of electronic chemical sensors with partial specificity and an appropriate pattern-recognition system, capable of recognising simple or complex odours'. There, partial specificity represents a universal hardware set that generates a fingerprint to represent a unique response to an analyte or class of analytes. Furthermore, equal emphasis is placed on the pattern-recognition system interpreting ensuing information as much as the hardware, highlighting the importance of signal processing and other analytical techniques in interpreting the complex signals of any hardware system seeking to emulate a neurobiological pathway. Successful implementation of a sensor system should give accurate classification and quantitation of the subject analyte, or the concentration of its constituent volatiles, as determined by its application [197, 223, 234–237].

The propensity of sensor materials to drift, in olfaction-inspired systems and others, motivates the use of compensatory techniques at the preprocessing and pattern recognition stages. These modifications are intended to to make the overall system response more reproducible over time. Drift is a well-studied and active area of research in sensing, as the instability of sensor materials may pose a serious barrier to widespread adoption [238, 239]. When drift in a sensor system is well-understood and quantified, corrective measures may be incorporated at the preprocessing stage using relative or differential baseline manipulations [240]. More often than not, however, the inherent nonlinearity of sensor data introduced by drift is hard to quantify. This has led to the widespread adoption of nonparametric pattern recognition techniques, particularly artificial neural networks like self-organizing maps (SOMs) [241] for data compression and multilayer perceptrons (MLPs) for classification [242, 243].

Artificial neural networks (ANNs) provide a number of advantages including adaptability in terms of training, self-organization, inherent parallelism, and noise tolerance. These advantages are compounded by hardware and software advances in recent years, which have made ANNs even more powerful and easy to use. The primary setback of this approach is that data encoded within the neural network can be difficult to understand and relate to an intuitive explanation. In addition, ANNs require large datasets to perform reliably which are not always readily available for chemore-

sistive platforms, especially in experimental settings. In those cases, classification techniques such as SVMs, logistic regression, and decision trees may serve as useful starting points in building intuition. The type and architectural specifics of the ANN is a matter of design left to the researcher, but very commonly is made up of a shallow network of multilayer perceptrons, represented by four or less hidden layers. The number of hidden layers was found to have no great improvement on the accuracy [244–246] and recent studies by computational neuroscientists seem to confirm this representation of olfactory system [247, 248], having shallow but sparse neural networks with multiple subunits that map data from the input layer proportionately. That being said, some studies have also employed deep neural networks inspired by the constitution of the visual system with success [249–251].

7. Conclusions

Both 2D materials and data analytics—mainly by virtue of hardware and software advances in machine learning—appear to have reached inflection points in recent years. This review makes the case for an intersection of fields through the use of 2D materials in the development of chemical sensor systems. A variety of 2D materials were surveyed including graphene as a 2D semi-metal, transition metal dichalcogenides (TMDs) as 2D semiconductors, and metal-oxide semiconductors (MOX) as thin film semiconductors. Key material attributes relevant to chemical sensing have been highlighted for each of the materials along with more practical concerns such as the current status in synthesis techniques. Graphene and MOX are presented as more mature materials, while TMDs are presented as a less mature from a material synthesis point of view. TMDs, however, offer a bandgap (as opposed to graphene), which may enable enhanced sensitivity and better scalability in terms of building multi-device sensor arrays.

2D and thin film materials are promising for chemical sensing applications owing primarily to their high surface-to-volume ratio. This holds true and may be exploited in various types of chemical sensors including optics-based chemical sensors, electrochemical sensors, and FET-based chemical sensors. General operation mechanisms have been detailed for each sensor type along with its unique set of advantages and setbacks. Optical sensors are unique in that they may not disturb chemical environments through measurement or require the manufacture of complex array structures. They do, however, pose difficulties in terms of miniaturization and cost. As a result, this review focuses on FET-based chemical sensors for their ability to combine the sensing capabilities of electrochemical sensors with scalability features similar to CMOS for the construction of large arrays. FET-based sensors are intended to also include chemiresistive sensors, which are treated as a two-terminal variant of FET-based sensors.

The core performance metrics related to sensor systems such as sensitivity, selectivity, response time, and stability are briefly summarized and presented in the context of 2D materials. This was included to encourage a more practical and holistic viewpoint on sensor performance. From there, the development of FET-based sensor arrays for fingerprinting complex chemical environments is motivated. Advantages of FET-based sensors are outlined while highlighting the importance of accurate device models for performance optimization and readout circuitry design. Lastly, various data processing techniques are summarized. These include methods for data compression/feature extraction, cluster analysis, and model classification. Special emphasis is given to olfaction-inspired sensor systems to motivate the use of data analysis techniques such as machine learning, which provide a number of advantages including adaptability in terms of training, self-organization, inherent parallelism, and noise tolerance.

Acknowledgments

Mantian Xue, Yuxuan Lin, and Tomás Palacios would like to acknowledge the partial support of the Army-MIT Institute for Soldier Nanotechnologies, the NSF Center for Integrated Quantum Materials, and the AFOSR FATE MURI.

ORCID iDs

Charles Mackin https://orcid.org/0000-0001-8413-5583
Yuxuan Lin https://orcid.org/0000-0003-0638-2620

References

[1] Mordor Intelligence 2018 *Technical Report* Global Chemical Sensor Market—Segmented by Product Type, End-user Industry (Industrial, Medical, Environmental Monitoring, and Defense and Homeland Security), and Region—Growth, Trends, and Forecast (2018–2023)
[2] Kumar R 2018 Global Sensor Market by Type, Technology, and End User: Global Opportunity Analysis and Industry Forecast, 2017–2025 *Technical Report* (Applied Market Research)
[3] Rothberg J M *et al* 2011 *Nature* **475** 348–52
[4] Tavira B, Gómez J, Santos F, Gil H, Alvarez V and Coto E 2014 *J. Hum. Genet.* **59** 376–80
[5] Ley T J *et al* 2008 *Nature* **456** 66–72
[6] Andries K *et al* 2010 *Science* **307** 223–7
[7] Insel T R, Landis S C and Collins F S 2013 *Science* **340** 687–8
[8] Koroshetz W *et al* 2018 *J. Neurosci.* **38** 6427–38
[9] Griller S, Ip N, Koch C, Koroshetz W, Okano H, Polachek M, Poo M M and Sejnowski T 2016 *Nat. Neurosci.* **19** 1118–22
[10] Anderson D J *et al* 2015 *Phil. Trans. R. Soc.* B **370** 20140164
[11] Vieira N C, Borme J, MacHado G, Cerqueira F, Freitas P P, Zucolotto V, Peres N M and Alpuim P 2016 *J. Phys.: Condens. Matter* **28** 085302
[12] Lerner B *et al* 2016 *Sensors Actuators* B **239** 1261–7
[13] Shue A *et al* 2019 *Sci. Rep.* **9** 434
[14] Scarselli M, Castrucci P and De Crescenzi M 2012 *J. Phys.: Condens. Matter* **24** 313202

[15] Wu M H, Li L, Liu N, Wang D J, Xue Y C and Tang L 2018 *Process Saf. Environ. Prot.* **118** 40–58
[16] Schleife A, Varley J B, Fuchs F, Rödl C, Bechstedt F, Rinke P, Janotti A and Van de Walle C G 2011 *Phys. Rev.* B **83** 035116
[17] Mackin C, Schroeder V, Zurutuza A, Su C, Kong J, Swager T M and Palacios T 2018 *ACS Appl. Mater. Interfaces* **10** 16169–76
[18] Madhavan A and Ng Y 2009 Large-scale deep unsupervised learning using graphics processors *26th Int. Conf. on Machine Learning* pp 873–80
[19] Bojarski M, Yeres P, Choromanska A, Choromanski K, Firner B, Jackel L and Muller U 2017 (arXiv:1704.07911)
[20] Chen M C, Ball R L, Yang L, Moradzadeh N, Chapman B E, Larson D B, Langlotz C P, Amrhein T J and Lungren M P 2017 *Radiology* **286** 845–52
[21] Selvikvåg Lundervold A and Lundervold A 2018 *Z. Med. Phys.* **29** 102–27
[22] LeCun Y, Bengio Y and Hinton G 2015 *Nature* **521** 436–44
[23] He K, Zhang X, Ren S and Sun J 2015 (arXiv:1502.01852)
[24] Silver D *et al* 2016 *Nature* **529** 484–9
[25] Geim A K and Novoselov K S 2007 *Nature* **6** 183–91
[26] Akhtar M, Anderson G, Zhao R, Alruqi A, Mroczkowska J E, Sumanasekera G and Jasinski J B 2017 *npj 2D Mater. Appl.* **1** 5
[27] Zhu B Y, Murali S, Cai W, Li X, Suk J W, Potts J R and Ruoff R S 2010 *Adv. Mater.* **22** 3906–24
[28] Soldano C, Mahmood A and Dujardin E 2010 *Carbon* **48** 2127–50
[29] Gruber E *et al* 2016 *Nat. Commun.* **7** 13948
[30] Takeuchi K *et al* 2017 *J. Phys. Chem.* C **121** 2807–14
[31] Ohta T, Bostwick A, McChesney J L, Seyller T, Horn K and Rotenberg E 2007 *Phys. Rev. Lett.* **98** 16–9
[32] Reina A, Jia X, Ho J, Nezich D, Son H, Bulovic V, Dresselhaus M S and Jing K 2009 *Nano Lett.* **9** 30–5
[33] Lin C 2009 *Nat. Nanotechnol.* **4** 212–3
[34] Fang W, Hsu A L, Song Y, Birdwell A G, Amani M, Dubey M, Dresselhaus M S, Palacios T and Kong J 2014 *ACS Nano* **8** 6491–9
[35] Fang W, Hsu A L, Song Y and Kong J 2015 *Nanoscale* **7** 20335–51
[36] Schedin F, Geim A K, Morozov S V, Hill E W, Blake P, Katsnelson M I and Novoselov K S 2007 *Nat. Mater.* **6** 652–5
[37] Novoselov K S, Geim A K, Morozov S V, Jiang D, Katsnelson M I, Grigorieva I V, Dubonos S V and Firsov A A 2005 *Nature* **438** 197–200
[38] Plochocka P, Faugeras C, Orlita M, Sadowski M L, Martinez G, Potemski M, Goerbig M O, Fuchs J N, Berger C and de Heer W A 2008 *Phys. Rev. Lett.* **100** 087401
[39] Abergel D S L, Apalkov V, Berashevich J, Ziegler K and Chakraborty T 2010 *Adv. Phys.* **59** 261–482
[40] Dash G N, Pattanaik S R and Sriyanka B 2014 *IEEE J. Electron Devices Soc.* **2** 77–104
[41] Ando T 2009 *NPG Asia Mater.* **1** 17–21
[42] Geim A K 2009 *Science* **324** 1530–4
[43] Wang R, Wang S, Zhang D, Li Z, Fang Y and Qiu X 2010 *ACS Nano* **5** 408–12
[44] Avouris P 2010 *Nano Lett.* **10** 4285–94
[45] Schulz M J, Shanov V N and Yin Z 2014 Transition from tubes to Sheets—a comparison of the properties and applications of carbon nanotubes and graphene *Nanotube Superfiber Materials: Changing Engineering Design* 1st edn ch 19, pp 519–68
[46] Castro Neto A H, Guinea F, Peres N M R, Novoselov K S and Geim A K 2009 *Rev. Mod. Phys.* **81** 109–62
[47] Wang H, Zhao H, Hu G, Li S, Su H and Zhang J 2015 *Sci. Rep.* **5** 18258
[48] Mackin C, McVay E and Palacios T 2018 *Sensors* **18** 494
[49] Petrone N, Dean C R, Meric I, Van Der Zande A M, Huang P Y, Wang L, Muller D, Shepard K L and Hone J 2012 *Nano Lett.* **12** 2751–6
[50] Bolotin K I, Sikes K J, Jiang Z, Klima M, Fudenberg G, Hone J, Kim P and Stormer H L 2008 *Solid State Commun.* **146** 351–5
[51] Lemme M C, Member S, Echtermeyer T J, Baus M and Kurz H 2007 *IEEE Electron Device Lett.* **28** 282–4
[52] Lemme M C, Echtermeyer T J, Baus M, Szafranek B N, Bolten J, Schmidt M, Wahlbrink T and Kurz H 2008 *Solid-State Electron.* **52** 514–8
[53] Wang H, Hsu A, Wu J, Kong J and Palacios T 2010 *IEEE Electron Device Lett.* **31** 906–8
[54] Wang H, Taychatanapat T, Hsu A, Watanabe K, Taniguchi T, Jarillo-Herrero P and Palacios T 2011 *IEEE Electron Device Lett.* **32** 1209–11
[55] Xu H, Zhang Z, Xu H, Wang Z, Wang S and Peng L M 2011 *ACS Nano* **5** 5031–7
[56] Hopf T, Vassilevski K V, Escobedo-Cousin E, King P J, Wright N G, O'Neill A G, Horsfall A B, Goss J P, Wells G H and Hunt M R 2014 *J. Appl. Phys.* **116** 154504
[57] Lin Y M, Jenkins K, Farmer D, Valdes-Garcia A, Avouris P, Sung C Y, Chiu H Y and Ek B 2009 Development of graphene FETs for high frequency electronics *IEEE Int. Electron Devices Meeting* pp 237–40
[58] Han S J, Jenkins K A, Valdes Garcia A, Franklin A D, Bol A A and Haensch W 2011 *Nano Lett.* **11** 3690–3
[59] Liao L and Duan X 2012 *Mater. Today* **15** 328–38
[60] Fu W, Feng L, Panaitov G, Kireev D, Mayer D, Offenhausser A and Krause H-J 2017 *Sci. Adv.* **3** e1701247
[61] Balandin A A 2013 *Nat. Nanotechnol.* **8** 549–55
[62] Masvidal-Codina E *et al* 2019 *Nat. Mater.* **18** 280–8
[63] Elias D C *et al* 2009 *Science* **323** 610–4
[64] Wang X, Zhi L and Muellen K 2008 *Nano Lett.* **8** 323–7
[65] Hess L H, Hauf M V, Seifert M, Speck F, Seyller T, Stutzmann M, Sharp I D and Garrido J A 2011 *Appl. Phys. Lett.* **99** 033503
[66] Stoller M D, Magnuson C W, Zhu Y, Murali S, Suk J W, Piner R and Ruoff R S 2011 *Energy Environ. Sci.* **4** 4685–9
[67] Ji H, Zhao X, Qiao Z, Jung J, Zhu Y, Lu Y, Zhang L L, MacDonald A H and Ruoff R S 2014 *Nat. Commun.* **5** 3317
[68] Chen D, Tang L and Li J 2010 *Chem. Soc. Rev.* **39** 3157–80
[69] Brownson D A, Kampouris D K and Banks C E 2012 *Chem. Soc. Rev.* **41** 6944–76
[70] Xia J, Chen F, Li J and Tao N 2009 *Nat. Nanotechnol.* **4** 505–9
[71] Zhou M, Zhai Y and Dong S 2009 *Anal. Chem.* **81** 5603–13
[72] Hess L H, Seifert M and Garrido J A 2013 *Proc. IEEE* **101** 1780–92
[73] Lee J U, Yoon D and Cheong H 2012 *Nano Lett.* **12** 4444–8
[74] Lee C, Kysar J W and Hone J 2008 *Science* **321** 385–9
[75] Kwak Y H, Choi D S, Kim Y N, Kim H, Yoon D H, Ahn S S, Yang J W, Yang W S and Seo S 2012 *Biosens. Bioelectron.* **37** 82–7
[76] Yoon H J, Zhang Y, Kim S S, Cheng M M C and Zhou Z 2011 A flexible biocompatible graphene sensor for real-time monitoring of pH and protein *6th IEEE Int. Conf. on Nano/Micro Engineered and Molecular Systems* (IEEE) pp 1104–7
[77] Song Y, Kong J, Martins L G P, Dresselhaus M S, Zeng T and Araujo P T 2013 *Proc. Natl Acad. Sci.* **110** 17762–7
[78] Kim K S, Zhao Y, Jang H, Lee S Y, Kim J M, Kim K S, Ahn J H, Kim P, Choi J Y and Hong B H 2009 *Nature* **457** 706–10
[79] Nair R R, Blake P, Grigorenko A N, Novoselov K S, Booth T J, Stauber T, Peres N M R and Geim A K 2008 *Science* **320** 1308
[80] Park D W *et al* 2014 *Nat. Commun.* **5** 5258
[81] Garrido J A *et al* 2017 *Adv. Funct. Mater.* **28** 1703976
[82] Lu Y, Liu X and Kuzum D 2018 *Curr. Opin. Biomed. Eng.* **6** 138–47
[83] Qiang Y *et al* 2019 *Sci. Adv.* **4** eaat0626
[84] Zhang Y, Tan Y W, Stormer H L and Kim P 2005 *Nature* **438** 201–4
[85] Ghosh S, Calizo I, Teweldebrhan D, Pokatilov E P, Nika D L, Balandin A A, Bao W, Miao F and Lau C N 2008 *Appl. Phys. Lett.* **92** 151911
[86] Teweldebrhan D, Lau C N, Ghosh S, Balandin A A, Bao W, Calizo I, Miao F and Lau C N 2008 *Nano Lett.* **8** 902–7
[87] Borovikov V and Zangwill A 2009 *Phys. Rev.* B **80** 121406
[88] de Heer W A, Berger C, Ruan M, Sprinkle M, Li X, Hu Y, Zhang B, Hankinson J and Conrad E 2011 *Proc. Natl Acad. Sci. USA* **108** 16900–5
[89] Hertel S, Waldmann D, Jobst J, Albert A, Albrecht M, Reshanov S, Schöner A, Krieger M and Weber H B 2012 *Nat. Commun.* **3** 957

[90] Bhaviripudi S, Jia X, Dresselhaus M S and Kong J 2010 *Nano Lett.* **10** 4128–33
[91] Yang W, Ratinac K R, Ringer S R, Thordarson P, Gooding J J and Braet F 2010 *Angew. Chem.* **49** 2114–38
[92] El-Kady M F, Veronica S, Sergey D and Richard B K 2012 *Science* **335** 1326–30
[93] Özyilmaz B *et al* 2010 *Nat. Nanotechnol.* **5** 574–8
[94] Losurdo M, Giangregorio M M, Capezzuto P and Bruno G 2011 *Phys. Chem. Chem. Phys.* **13** 20836–43
[95] Song Y, Fang W, Hsu A L and Kong J 2014 *Nanotechnology* **25** 395701
[96] Shen P C, Lin Y, Wang H, Park J H, Leong W S, Lu A Y, Palacios T and Kong J 2018 *IEEE Trans. Electron Devices* **65** 4040–52
[97] Kim K K, Reina A, Olmos-Asar J A, Mankey G J, Negreiros F R, Araujo P T, Mafra D L, Kong J and Dresselhaus M S 2018 *Phys. Rev. Mater.* **2** 073404
[98] Wang Y, Zheng Y, Xu X, Dubuisson E, Bao Q, Lu J and Loh K P 2011 *ACS Nano* **5** 9927–33
[99] Cheng H M *et al* 2012 *Nat. Commun.* **3** 697–9
[100] Manzeli S, Ovchinnikov D, Pasquier D, Yazyev O V and Kis A 2017 *Nat. Rev. Mater.* **2** 17033
[101] Chhowalla M, Liu Z, Zhang H and Jacobs D H 2015 *Chem. Soc. Rev.* **44** 2584–6
[102] Pauling L and Dickinson R G 1923 *J. Am. Chem. Soc.* 45 1466–71
[103] Joensen P, Frindt R F and Morrison S R 1986 *Mater. Res. Bull.* **21** 457–61
[104] Choi W, Choudhary N, Han G H, Park J, Akinwande D and Lee Y H 2017 *Mater. Today* **20** 116–30
[105] Han G H, Duong D L, Keum D H, Yun S J and Lee Y H 2018 *Chem. Rev.* **118** 6297–336
[106] Zhou X, Cheng J, Zhou Y, Cao T, Hong H, Liao Z, Wu S, Peng H, Liu K and Yu D 2015 *J. Am. Chem. Soc.* **137** 7994
[107] Zhang J, Peng Z, Soni A, Zhao Y, Xiong Y, Peng B, Wang J, Dresselhaus M S and Xiong Q 2011 *Nano Lett.* **11** 2407–14
[108] Gan X, Lee L Y S, Wong K Y, Lo T W, Ho K H, Lei D Y and Zhao H 2018 *ACS Appl. Energy Mater.* **1** 4754–65
[109] Sokolikova M S, Sherrell P C, Palczynski P, Bemmer V L and Mattevi C 2019 *Nat. Commun.* **10** 712
[110] Bissessur R, Kanatzidis M G, Schindlerb J L and Kannewurfb C R 1993 *J. Chem. Soc. Chem. Commun.* **20** 1582–5
[111] Hill H M, Rigosi A F, Rim K T, Flynn G W and Heinz T F 2016 *Nano Lett.* **16** 4831–7
[112] Wang H, Yu L, Lee Y H, Shi Y, Hsu A, Chin M L, Li L J, Dubey M, Kong J and Palacios T 2012 *Nano Lett.* **12** 4674–80
[113] Yu L *et al* 2014 *Nano Lett.* **14** 3055–63
[114] Yu L, Zubair A, Santos E J, Zhang X, Lin Y, Zhang Y and Palacios T 2015 *Nano Lett.* **15** 4928–34
[115] Yu Z *et al* 2016 *Adv. Mater.* **28** 547–52
[116] Nam H, Oh B R, Chen P, Chen M, Wi S, Wan W, Kurabayashi K and Liang X 2015 *Sci. Rep.* **5** 10546
[117] Li X, Mullen J T, Jin Z, Borysenko K M, Nardelli M B and Kim K W 2013 *Phys. Rev.* B **87** 115418
[118] Kaasbjerg K, Thygesen K S and Jauho A P 2013 *Phys. Rev.* B **87** 235312
[119] Zhang W, Huang Z, Zhang W and Li Y 2014 *Nano Res.* **7** 1731–7
[120] Radisavljevic B and Kis A 2013 *Nat. Mater.* **12** 815–20
[121] Park M, Park Y J, Chen X, Park Y K, Kim M S and Ahn J H 2016 *Adv. Mater.* **28** 2556–62
[122] Castellanos-Gomez A, Poot M, Steele G A, Van Der Zant H S, Agraït N and Rubio-Bollinger G 2012 *Adv. Mater.* **24** 772–5
[123] Bertolazzi S, Brivio J and Kis A 2011 *ACS Nano* **5** 9703–9
[124] Arthur J R 2002 *Surf. Sci.* **500** 189–217
[125] Kwon H, Garg S, Park J H, Jeong Y, Yu S, Kim S M, Kung P and Im S 2019 *npj 2D Mater. Appl.* **3** 1–9
[126] Cheon J, Gozum J E and Girolami G S 1997 *Chem. Mater.* **9** 1847–53
[127] Kang K, Xie S, Huang L, Han Y, Huang P Y, Mak K F, Kim C J, Muller D and Park J 2015 *Nature* **520** 656–60
[128] Lin T W *et al* 2012 *Adv. Mater.* **24** 2320–5
[129] Chuang H J, Chamlagain B, Koehler M, Perera M M, Yan J, Mandrus D, Tománek D and Zhou Z 2016 *Nano Lett.* **16** 1896–902
[130] Ouyang B, Xiong S and Jing Y 2018 *npj 2D Mater. Appl.* **2** 13
[131] Korotcenkov G, Cornet A, Rossinyol E, Arbiol J, Brinzari V and Blinov Y 2005 *Thin Solid Films* **471** 310–9
[132] Franke M, Koplin T and Simon U 2006 *Small* **2** 36–50
[133] Brattain W H and Bardeen J 1953 *Bell Syst. Tech. J.* **32** 1–41
[134] Heiland G, Mollwo E and Stöckmann F 1959 *Solid State Phys.* 8 191–323
[135] Seiyama T, Kato A, Fujiishi K and Nagatani M 1962 *Anal. Chem.* **34** 1502–3
[136] Taguchi N 1962 A metal oxide gas sensor *JP Patent* 45–38200
[137] Taguchi N 1971 Method for making a gas-sensing element 1971 *US Patent* 3,625,756A
[138] Korotcenkov G 2007 *Mater. Sci. Eng.* B **139** 1–23
[139] Kim H J and Lee J H 2014 *Sensors Actuators* B **192** 607–27
[140] Das S and Jayaraman V 2014 *Prog. Mater. Sci.* **66** 112–255
[141] Yamazoe N, Sakai G and Shimanoe K 2003 *Catalysis Surv. Asia* **7** 63–75
[142] Barsan N and Weimar U 2001 *J. Electroceramics* **7** 143–67
[143] Korotcenkov G, Han S-D, Cho B K and Brinzari V 2009 *Crit. Rev. Solid State Mater. Sci.* **34** 1–17
[144] Korotcenkov G and Cho B 2009 *Sensors Actuators* B **142** 321–30
[145] Becker T, Ahlers S, Bosch-vBraunmhl C, Mller G and Kiesewetter O 2001 *Sensors Actuators* B **77** 55–61 (*Proc. of the 8th Int. Meeting on Chemical Sensors*)
[146] Gardner J W 1989 *Semicond. Sci. Technol.* **4** 345–50
[147] Sakai G, Matsunaga N, Shimanoe K and Yamazoe N 2001 *Sensors Actuators* B **80** 125–31
[148] Sberveglieri G 1992 *Sensors Actuators* B **6** 239–47
[149] Korotcenkov G, Brinzari V, Schwank J, DiBattista M and Vasiliev A 2001 *Sensors Actuators* B **77** 244–52
[150] Fasoli A, Lionti K, Sundberg L, Miller R D, Ceccarelli F and Bozano L 2017 Analysis of tin oxide thin films fabricated via sol-gel and delayed ignition of combustion processes *ISOCS/IEEE Int. Symp. on Olfaction and Electronic Nose (ISOEN)* pp 1–3
[151] Paulus G L *et al* 2014 *Sci. Rep.* **4** 6865
[152] Mackin C, Hess L H, Hsu A, Song Y, Kong J, Garrido J A and Palacios T 2014 *IEEE Trans. Electron Devices* **61** 3971–7
[153] Zhu A Y and Cubukcu E 2015 *2D Mater.* **2** 032005
[154] Farmer D B, Avouris P, Li Y, Heinz T F and Han S J 2016 *ACS Photonics* **3** 553–7
[155] Li Y, Yan H, Farmer D B, Meng X, Zhu W, Osgood R M, Heinz T F and Avouris P 2014 *Nano Lett.* **14** 1573–7
[156] Hu H, Yang X, Zhai F, Hu D, Liu R, Liu K, Sun Z and Dai Q 2016 *Nat. Commun.* **7** 12334
[157] Hu H, Yang X, Guo X, Khaliji K, Biswas S R, de Abajo F J G, Low T, Sun Z and Dai Q 2019 *Nat. Commun.* **10** 1131
[158] Ling X, Huang S, Deng S, Mao N, Kong J, Dresselhaus M S and Zhang J 2015 *Acc. Chem. Res.* **48** 1862–70
[159] Silver A, Kitadai H, Liu H, Granzier-Nakajima T, Terrones M, Ling X and Huang S 2019 *Nanomaterials* **9** 516
[160] Ling X, Xie L, Fang Y, Xu H, Zhang H, Kong J, Dresselhaus M S, Zhang J and Liu Z 2009 *Nano Lett.* **10** 553–61
[161] Ling X, Fang W, Lee Y H, Araujo P T, Zhang X, Rodriguez-Nieva J F, Lin Y, Zhang J, Kong J and Dresselhaus M S 2014 *Nano Lett.* **14** 3033–40
[162] Tongay S, Zhou J, Ataca C, Liu J, Kang J S, Matthews T S, You L, Li J, Grossman J C and Wu J 2013 *Nano Lett.* **13** 2831–6
[163] Mao N, Chen Y, Liu D, Zhang J and Xie L 2013 *Small* **9** 1312–5
[164] Mouri S, Miyauchi Y and Matsuda K 2013 *Nano Lett.* **13** 5944–8
[165] Lin Y, Ling X, Yu L, Huang S, Hsu A L, Lee Y H, Kong J, Dresselhaus M S and Palacios T 2014 *Nano Lett.* **14** 5569–76
[166] Zhu C, Du D and Lin Y 2015 *2D Mater.* **2** 032004
[167] Bard A J and Faulkner L R 2001 *Electrochemical Methods: Fundamentals and Applications* (New York: Wiley) pp 1–833
[168] Yan R, Qiu S, Tong L and Qian Y 2016 *Chem. Speciation Bioavailability* **28** 72–7
[169] He Q, Das S R, Garland N T, Jing D, Hondred J A, Cargill A A, Ding S, Karunakaran C and Claussen J C 2017 *ACS Appl. Mater. Interfaces* **9** 12719–27
[170] Wang Y, Li Y, Tang L, Lu J and Li J 2009 *Electrochem. Commun.* **11** 889–92
[171] Hou S, Kasner M L, Su S, Patel K and Cuellari R 2010 *J. Phys. Chem.* C **114** 14915–21

[172] Tan L, Zhou K G, Zhang Y H, Wang H X, Wang X D, Guo Y F and Zhang H L 2010 *Electrochem. Commun.* **12** 557–60
[173] Mallesha M, Manjunatha R, Nethravathi C, Suresh G S, Rajamathi M, Melo J S and Venkatesha T V 2011 *Bioelectrochemistry* **81** 104–8
[174] Mao Y, Bao Y, Gan S, Li F and Niu L 2011 *Biosens. Bioelectron.* **28** 291–7
[175] Wu L, Feng L, Ren J and Qu X 2012 *Biosens. Bioelectron.* **34** 57–62
[176] Qian T, Yu C, Zhou X, Wu S and Shen J 2014 *Sensors Actuators* B **193** 759–63
[177] Baraneedharan P 2016 *J. Nanomed. Res.* **3** 00066
[178] Xu G, Jarjes Z A, Desprez V, Kilmartin P A and Travas-Sejdic J 2018 *Biosens. Bioelectron.* **107** 184–91
[179] Yin R *et al* 2018 *Nat. Commun.* **9** 2334
[180] Liu X, Lu Y, Iseri E, Shi Y and Kuzum D 2018 *Frontiers Neurosci.* **12** 132
[181] Radisavljevic B, Whitwick M B and Kis A 2012 *Appl. Phys. Lett.* **101** 043103
[182] Sanne A, Park S, Ghosh R, Yogeesh M N, Liu C, Mathew L, Rao R, Akinwande D and Banerjee S K 2017 *npj 2D Mater. Appl.* **1** 26
[183] Fu W, Lima L M C, Jiang L, Schneider G F and van Geest E P 2016 *Adv. Mater.* **29** 1603610
[184] Mailly-Giacchetti B, Hsu A, Wang H, Vinciguerra V, Pappalardo F, Occhipinti L, Guidetti E, Coffa S, Kong J and Palacios T 2013 *J. Appl. Phys.* **114** 084505
[185] Zheng C, Jin X, Li Y, Mei J, Sun Y, Xiao M, Zhang H, Zhang Z and Zhang G J 2019 *Sci. Rep.* **9** 759
[186] Zhang M, Liao C, Mak C H, You P, Mak C L and Yan F 2015 *Sci. Rep.* **5** 8311
[187] Kostarelos K, Vincent M, Hebert C and Garrido J A 2017 *Adv. Mater.* **29** 1700909
[188] Xu S *et al* 2017 *Nat. Commun.* **8** 14902
[189] Lee J, Dak P, Lee Y, Park H, Choi W, Alam M A and Kim S 2014 *Sci. Rep.* **4** 7352
[190] Srinivasan K and Rechnitz G A 1969 *Anal. Chem.* **41** 1203–8
[191] Oesch U, Ammann D and Simon W 1986 *Clin. Chem.* **32** 1448–59
[192] Xuan P A G, Zheng G and Lieber C M 2010 *Nano Lett.* **10** 547–52
[193] Georgakilas V, Otyepka M, Bourlinos A B, Chandra V, Kim N, Kemp K C, Hobza P, Zboril R and Kim K S 2012 *Chem. Rev.* **112** 6156–214
[194] Bakker E, Bühlmann P and Pretsch E 1997 *Chem. Rev.* **97** 3083–132
[195] Lee A P and Reedy B J 1999 *Sensors Actuators* B **60** 35–42
[196] Vergara A, Llobet E, Brezmes J, Ivanov P, Can C, Grcia I, Vilanova X and Correig X 2007 *Sensors Actuators* B **123** 1002–16
[197] Leidinger M, Sauerwald T, Reimringer W, Ventura G and Schütze A 2014 *J. Sens. Sens. Syst.* **3** 253–63
[198] Martinelli E, Polese D, Catini A, DAmico A and Natale C D 2012 *Sensors Actuators* B **161** 534–41
[199] Korotcenkov G 2005 *Sensors Actuators* B **107** 209–32 (*Proc. of the 7th European Conf. on Optical Chemical Sensors and Biosensors*)
[200] Turner A, Chen B and Piletsky S 1999 *Clin. Chem. 45* 1596–601
[201] Heller A 1996 *Curr. Opin. Biotechnol.* **7** 50–4
[202] Korotcenkov G and Cho B 2011 *Sensors Actuators* B **156** 527–38
[203] Matsuura Y and Takahata K 1991 *Sensors Actuators* B **5** 205–9
[204] Yang G, Haibo Z and Biying Z 2000 *J. Mater. Sci.* **35** 917–23
[205] Albert K J, Lewis N S, Schauer C L, Sotzing G A, Stitzel S E, Vaid T P and Walt D R 2000 *Chem. Rev.* **100** 2595–626
[206] Mackin C and Palacios T 2016 *Analyst* **141** 2704–11
[207] Rabaey J M, Chandrakasan A and Nikolic B 2003 *Digital Integrated Circuits* (Upper Saddle River, NJ: Pearson) pp 623–720
[208] Sedra A S and Smith K C 2010 *Microelectronic Circuits* (Oxford: Oxford University Press) pp 1203–52
[209] Cho B *et al* 2015 *Sci. Rep.* **5** 8052
[210] Chiu S W and Tang K T 2013 *Sensors* **13** 14214–47
[211] Lee H, Lee S, Kim D H, Perello D, Park Y J, Hong S H, Yun M and Kim S 2012 *Sensors* **12** 2582–97
[212] Meric I, Han M Y, Young A F, Ozyilmaz B, Kim P and Shepard K L 2008 *Nat. Nanotechnol.* **3** 654–9
[213] Lu N, Wang W, Xu G, Jin Z, Li L, Ji Z, Wang L, Peng S and Liu M 2016 *J. Appl. Phys.* **120** 084509
[214] Radisavljevic B, Radenovic A, Brivio J, Giacometti V and Kis A 2011 *Nat. Nanotechnol.* **6** 147–50
[215] Yoon Y, Ganapathi K and Salahuddin S 2011 *Nano Lett.* **11** 3768–73
[216] Krasnozhon D, Lembke D, Nyffeler C, Leblebici Y and Kis A 2014 *Nano Lett.* **14** 5905–11
[217] Knobloch T, Rzepa G, Illarionov Y Y, Waltl M, Schanovsky F, Stampfer B, Furchi M M, Mueller T and Grasser T 2018 *IEEE J. Electron Devices Soc.* **6** 972–8
[218] Cao J, Peng S, Liu W, Wu Q, Li L, Geng D, Yang G, Ji Z, Lu N and Liu M 2018 *J. Appl. Phys.* **123** 064501
[219] Weimar U and Göpel W 1995 *Sensors Actuators* B **26** 13–8
[220] Barsan N, Simion C, Heine T, Pokhrel S and Weimar U 2010 *J. Electroceramics* **25** 11–9
[221] Nomani M W K, Kersey D, James J, Diwan D, Vogt T, Webb R A and Koley G 2011 *Sensors Actuators* B **160** 251–9
[222] Zhang Q, Tan L, Chen Y, Zhang T, Wang W, Liu Z and Fu L 2016 *Adv. Sci.* **3** 1600130
[223] Wilson A and Baietto M 2009 *Sensors* **9** 5099–148
[224] Gardner J W, Hines E L and Wilkinson M 1990 *Meas. Sci. Technol.* **1** 446
[225] Ema K, Yokoyama M, Nakamoto T and Moriizumi T 1989 *Sensors Actuators* **18** 291–6
[226] Gutierrez-Osuna R 2002 *IEEE Sens. J.* **2** 189–202
[227] Scott S M, James D and Ali Z 2006 *Microchimica Acta* **156** 183–207
[228] Eklöv T, Mårtensson P and Lundström I 1999 *Anal. Chim. Acta* **381** 221–32
[229] Kermani B G, Schiffman S S and Nagle H T 1999 *IEEE Trans. Biomed. Eng.* **46** 429–39
[230] Persaud K and Dodd G 1982 *Nature* **299** 352
[231] Schild D 1988 *Biophys. J.* **54** 1001–11
[232] Hubel D and Wiesel T 1962 *J. Physiol.* **160** 106–54
[233] Gardner J W and Bartlett P N 1994 *Sensors Actuators* B **18** 210–1
[234] Arshak K, Moore E, Lyons G M, Harris J and Clifford S 2004 *Sen. Rev.* **24** 181–98
[235] Gardner J W, Shin H W and Hines E L 2000 *Sensors Actuators* B **70** 19–24
[236] Wilson A D and Baietto M 2011 *Sensors* **11** 1105–76
[237] Loutfi A, Coradeschi S, Mani G K, Shankar P and Rayappan J B B 2015 *J. Food Eng.* **144** 103–11
[238] Holmberg M, Winquist F, Lundström I, Davide F, DiNatale C and D'Amico A 1996 *Sensors Actuators* B **36** 528–35
[239] Romain A C and Nicolas J 2010 *Sensors Actuators* B **146** 502–6
[240] Artursson T, Eklöv T, Lundström I, Mårtensson P, Sjöström M and Holmberg M 2000 *J. Chemometr.* **14** 711–23
[241] Zuppa M, Distante C, Siciliano P and Persaud K C 2004 *Sensors Actuators* B **98** 305–17
[242] Hines E, Llobet E and Gardner J 1999 *IEE Proc.* 146 297–310
[243] Srivastava A 2003 *Sensors Actuators* B **96** 24–37
[244] Holmberg M, Winquist F, Lundström I, Gardner J and Hines E 1995 *Sensors Actuators* B **27** 246–9
[245] Gardner J, Craven M, Dow C and Hines E 1998 *Meas. Sci. Technol.* **9** 120
[246] Adak M and Yumusak N 2016 *Sensors* **16** 304
[247] Stevens C F 2015 *Proc. Natl Acad. Sci.* **112** 9460–5
[248] Dasgupta S, Stevens C F and Navlakha S 2017 *Science* **358** 793–6
[249] Längkvist M and Loutfi A 2011 Unsupervised feature learning for electronic nose data applied to bacteria identification in blood *NIPS 2011 Workshop on Deep Learning and Unsupervised Feature Learning* pp 1–7
[250] Liu Q, Hu X, Ye M, Cheng X and Li F 2015 *Int. J. Intell. Syst.* **30** 907–22
[251] Peng P, Zhao X, Pan X and Ye W 2018 *Sensors* **18** 157